Electronic Supplementary Material (ESI) for New Journal of Chemistry.

Supporting information

A stereo-electronic interpretation of a challenging orthoamide Overman rearrangement rationalized by molecular modelling

Judith Juvin, [a] Victor Malherbe, [a] Marie-Charlotte Belhomme , [a] Stéphanie Castex, [a] Agathe Martinez, [a] Hassan Khartabil,* [a] and Arnaud Haudrechy* [a,b]

[a.] *Institut de Chimie Moléculaire de Reims, UMR 7312, SFR Condorcet FR CNRS 3417, F-51687 REIMS Cedex, France.*

[b.] *E-mail : arnaud.haudrechy@univ-reims.fr*

(Submitted to *New J. Chem.*)

Table of contents

General information

Solvents and chemicals used for the reactions were purchased from commercial suppliers and used without further purification unless otherwise stated. Anhydrous DMF was obtained from Acros Organics. Anhydrous methylene chloride was collected under argon on a Pure-Solv, Innovative Technology machine.

The reaction evolution was followed by TLC under alumina silica plates ALUGRAM Xtra SIL G/UV (254 nm), revealed under U.V. and/or with a vanillin solution (4.3 g vanillin, 125 mL EtOH, 1.25 mL H_2SO_4). Chromatography was performed on silica gel, particle's size 40-63 µm, unless otherwise stated.

HPLC purifications were performed on a Macherey-Nagel Silica VP Nucleodur column (100 Å, 5 µm, 10 x 250 mm) using a 10 min, 5 mL/min flow of 5% isopropanol in hexane. The detection was set at 230 nm.

^{1}H NMR and ^{13}C NMR spectra were recorded on Bruker Avance 500 MHz and 600 MHz spectrometers. Observed chemical shift (δ) values are given in ppm and coupling constants (J) in Hz. ^{1}H NMR and ^{13}C NMR chemical shifts were calibrated using residual solvent signals at the following values: $CDCl_3$ δ H 7.27 ppm and δ C 77.16, DMSO-d_6 δ H 2.50 and δ C 39.52. The multiplicities have been described as followed: s (singlet), d (doublet), dd (doublet of doublet), dt (doublet of triplet), t (triplet), m (multiplet), br s (broad singlet) …

High Resolution Mass Spectra (HRMS) were recorded on a Waters SYNAPT G2-Si High Resolution Mass Spectrometry equipped with an electrospray ionization (ESI) source (Waters Corp., Manchester, UK).

Infrared spectra (IR) were recorded on a Spectrum 2 (Perkin-Elmer) spectroscope equipped with a UATR Two module.

Optical rotations were measured on a MCP 5100 (Anton Paar) polarimeter equipped with Hastelloy ToolMaster WL LÜR tubes (100 mm, for a 0.7 mL volume).

$[\alpha]_D^{20°C}$ were expressed in 10^{-1}.°.cm^2.g^{-1} units.

Synthetic procedures and characterization data for all new compounds

Synthesis of starting material 14

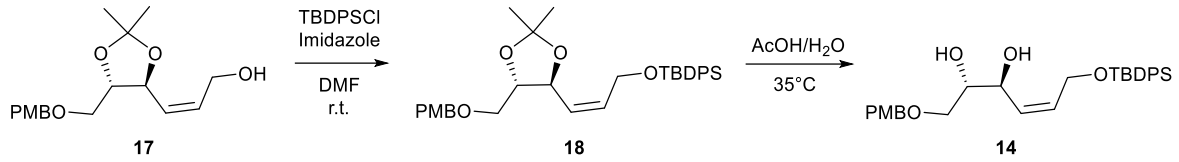

(2*Z*)-2,3-dideoxy-6-*O*-[(4-methoxyphenyl)methyl]-4,5-*O*-(1-methylethylidene)-1-*O*-(*tert*-butyldiphenylsilyl)-L-*threo*-hex-2-enitol **18**

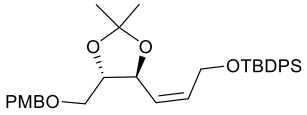

To a solution of allylic alcohol **17** (Y. Nakayama, R. Sekiya, H. Oishi, N. Hama, M. Yamazaki, T. Sato, N. Chida, *Chem. Eur. J.*, 2013, **19**, 12052) (200 mg, 0.65 mmol, 1.0 eq.) in DMF (640 µL), at room temperature under argon, were successively added imidazole (97 mg, 1.43 mmol, 2.2 eq.) and TBDPSCl (186 µL, 0.71 mmol, 1.1 eq.). The solution was stirred at room temperature for 80 min. The reaction was quenched by addition of aqueous solution of hydrochloric acid (3 mL, C = 1 M). The mixture was extracted with diethyl ether (3 x 8 mL). Combined organic phases were washed with brine (3 x 10 mL), dried over anhydrous $MgSO_4$, filtered and concentrated under reduced pressure. The desired product **18** (267 mg, 0.49 mmol, 75%) was obtained as a yellow oil after purification by chromatography on silica gel (petroleum ether/acetone: 100/0 to 90/10).

^{1}H NMR (500 MHz, $CDCl_3$): δ 7.68-7.66 (4 H, m), 7.44-7.41 (2 H, m), 7.40-7.36 (4 H, m), 7.15 (2 H, d, *J* = 8.6 Hz), 6.80 (2 H, d, *J* = 8.6 Hz), 5.88-5.83 (1 H, m), 5.48-5.43 (1 H, m), 4.43-4.39 (1 H, m), 4.38 (2 H, s), 4.33 (1 H, ddd, *J* = 13.5, 6.6, 1.5 Hz), 4.21 (1 H, ddd, *J* = 13.5, 5.6, 1.6 Hz), 3.81-3.77 (1 H, m), 3.79 (3 H, s), 3.43 (1 H, dd, *J* = 10.6, 3.3 Hz), 3.38 (1 H, dd, *J* = 10.6, 5.5 Hz), 1.40 (3 H, s), 1.36 (3 H, s), 1.05 (9 H, s). ^{13}C NMR (125 MHz, $CDCl_3$): δ 159.3, 135.7, 134.9, 133.7, 133.6, 130.1, 129.8, 129.4, 127.9, 127.1, 113.8, 109.5, 80.3, 73.9, 73.3, 69.1, 60.4, 55.4, 27.2, 27.1, 26.9, 19.3. ν_{max}/cm^{-1}: 2932, 2857, 1613, 1513, 1246, 1075, 820, 701, 503. HRMS (ESI): $[M+Na]^+$ calculated for $C_{33}H_{42}O_5NaSi$: 569.2699; found : 569.2702.

$[\alpha]_D^{20°C}$ = + 16.8 (c = 1.30, $CHCl_3$).

(2*Z*)-2,3-dideoxy-6-*O*-[(4-methoxyphenyl)methyl]-1-*O*-(*tert*-butyldiphenylsilyl)-L-*threo*-hex-2-enitol **14**

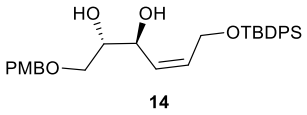

The starting material **18** (3.22 g, 5.89 mmol) was dissolved in AcOH/H_2O (4/1; 20 mL). The solution was stirred at 35°C for 41h. The product **14** (1.24 g, 2.45 mmol, 42%) was obtained as a colorless oil after concentration under reduced pressure and purification by chromatography on silica gel (petroleum ether/ethyl acetate: 100/0 to 60/40).

^{1}H NMR (500 MHz, $CDCl_3$): δ 7.69-7.67 (4 H, m), 7.46-7.37 (6 H, m), 7.17 (2 H, d, *J* = 8.5 Hz), 6.84 (2 H, d, *J* = 8.5 Hz), 5.80 (1 H, dddd, *J* = 11.3, 6.5, 5.7, 0.8 Hz), 5.49 (1 H, ddt, *J* = 11.3, 8.6, 1.4 Hz), 4.37 (2 H, s), 4.34 (1 H, ddd, *J* = 13.5, 6.9, 1.5 Hz), 4.27-4.21 (2 H, m), 3.80 (3 H, s), 3.58-3.54 (1 H, m), 3.48 (1 H, dd, *J* = 9.8, 3.5 Hz), 3.36 (1 H, dd, *J* = 9.8, 5.5 Hz), 2.59-2.58 (1 H, m), 2.53 (1 H, br s), 1.05 (9 H, s). ^{13}C

NMR (125 MHz, $CDCl_3$): δ 159.5, 135.7, 134.8, 133.7, 133.6, 130.1, 129.8, 129.4, 127.9, 127.1, 113.8, 109.5, 80.3, 73.9, 73.3, 69.1, 60.4, 55.4, 27.2, 27.1, 26.9, 19.3. ν_{max}/cm^{-1}: 3412, 3071, 2931, 2857, 1613, 1513, 1247, 1106, 1035, 820, 701, 503. HRMS (ESI): $[M+Na]^+$ calculated for $C_{30}H_{38}O_5NaSi$: 529.2386; found : 529.2392.

$[\alpha]_D^{25°C}$ = + 13.0 (c = 1.16, $CHCl_3$).

Synthesis of Overman product 13

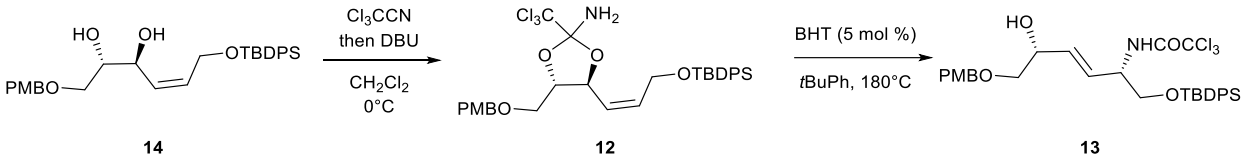

14 **12** **13**

(2*Z*)-2,3-dideoxy-6-*O*-[(4-methoxyphenyl)methyl]-4,5-*O*-[2,2,2-trichloroethylidene-1-amino]-1-*O*-(*tert*-butyldiphenylsilyl)-L-*threo*-hex-2-enitol (**12**)

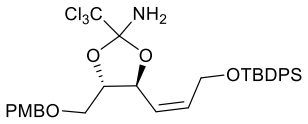

12

To a solution of diol **14** (878 mg, 1.73 mmol, 1.0 eq.) in methylene chloride (50 mL), at 0°C under argon, were successively added trichloroacetonitrile (230 µL, 2.29 mmol, 1.3 eq.) and 1,8-diazabicyclo[5.4.0]undec-7-ene (25 µL, 0.173 mmol, 0.1 eq.). This solution was stirred at 0°C for 6h30, then allowed to warm up to room temperature and concentrated under reduced pressure. The crude mixture (dr = 1:1) was purified by silica gel column chromatography (petroleum ether/ethyl acetate 100/0 to 70/30) to afford the two diastereoisomers of **12** (764 mg, 1.17 mmol, 68%, dr = 1:1) as a colorless oil. For analytical samples, the two diastereoisomers were separated by HPLC (less polar diastereoisomer: TR = 4.31 min, polar diastereoisomer: TR = 5.87 min).

Less polar diastereoisomer: ^{1}H NMR (600 MHz, DMSO-d_6): δ 7.65-7.59 (4 H, m), 7.49-7.42 (6 H, m), 7.11 (2 H, d, *J* = 8.5 Hz), 6.79 (2 H, d, *J* = 8.5 Hz), 5.90-5.86 (1 H, m), 5.55-5.52 (1 H, m), 4.89 (1 H, t, *J* = 8.8 Hz), 4.39 (1 H, ddd, *J* = 13.8, 6.7, 1.0 Hz), 4.32-4.23 (3 H, m), 4.08 (1 H, dt, *J* = 8.9, 4.5 Hz), 3.71 (3 H, s), 3.44 (2 H, d, *J* = 4.6 Hz), 3.24 (2 H, s), 0.98 (9 H, s). ^{13}C NMR (150 MHz, DMSO-d_6): δ 158.7, 135.2, 135.0, 130.0, 129.6, 129.3, 128.0, 127.9, 124.9, 115.8, 113.6, 103.5, 82.6, 79.2, 75.0, 72.1, 68.4, 60.0, 55.0, 26.6, 18.7. $[\alpha]_D^{20°C}$ = - 1.4 (c = 0.80, $CHCl_3$).

Polar diastereoisomer: ^{1}H NMR (600 MHz, DMSO-d_6): δ 7.62-7.58 (4 H, m), 7.48-7.37 (6 H, m), 7.11 (2 H, d, *J* = 8.5 Hz), 6.80 (2 H, d, *J* = 8.5 Hz), 5.87-5.83 (1 H, m), 5.60-5.57 (1 H, m), 4.75 (1 H, t, *J* = 8.9 Hz), 4.34-4.28 (3 H, m), 4.22 (1 H, *J* = 8.9, 5.3, 3.7 Hz), 4.15 (1 H, ddd, *J* = 13.6, 5.7, 0.8 Hz), 3.71 (3 H, s), 3.44 (2 H, m), 3.36 (2 H, s), 0.97 (9 H, s). ^{13}C NMR (150 MHz, DMSO-d_6): δ 158.7, 135.0, 134.2, 132.9, 132.7, 130.0, 129.9, 129.0, 128.0, 127.9, 126.9, 115.7, 113.5, 103.4, 80.5, 76.7, 72.0, 67.3, 59.8, 55.0, 26.6, 18.7. $[\alpha]_D^{20°C}$ = + 4.6 (c = 0.80, $CHCl_3$).

Mixture of diastereoisomers: ν_{max}/cm^{-1}: 3417, 3340, 3071, 2931, 2857, 1610, 1513, 1428, 1248, 1078, 821, 703. HRMS (ESI): $[M+Na]^+$ calculated for $C_{32}H_{38}NO_5NaSiCl_3$: 672.1483; found: 672.1495.

(3*E*)-2-[(2,2,2-trichloroacetyl)-amino]-2,3,4-trideoxy-6-*O*-[(4-methoxyphenyl)methyl]-1-*O*-(*tert*-butyldiphenylsilyl)-L-*threo*-hex-3-enitol (**13**)

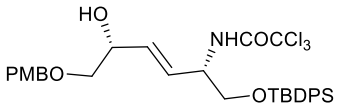

13

Procedure under classical heating. To a solution of the two diastereoisomers **12** (dr = 1:1, 24 mg, 0.037 mmol, 1 eq.) in *t*BuPh (1.36 mL) was added a solution (68 µL, C = 0.027 M) of 2,6-di-*tert*-butyl-4-methylphenol (BHT, 0.05 eq.) in *t*BuPh. The reaction mixture was purged with argon during 20 min, then heated at 180°C for 27h in a sealed tube. After cooling-down to room temperature, direct purification by chromatography on silica gel (pentane/ethyl acetate: 100/0 to 40/60) gave **13** (5 mg, 7.68 µmol, 21%) as a slightly yellow oil.

Procedure under microwave irradiation. To a solution of the two diastereoisomers **12** (dr = 1:1, 100 mg, 0.154 mmol, 1.0 eq.) in *t*BuPh (5.66 mL) was added a solution (284 µL, C = 0.027 M) of 2,6-di-*tert*-butyl-4-methylphenol (BHT, 0.05 eq.) in *t*BuPh. The reaction mixture was purged with argon during 20 min, then heated at 180°C during 4h under microwave irradiation (Discover S-Class, CEM Corporation – 250W). After cooling-down to room temperature, direct purification by chromatography on silica gel (pentane/ethyl acetate: 100/0 to 0/100) gave **13** (36 mg, 55.30 µmol, 36%) as a slightly yellow oil.

^{1}H NMR (600 MHz, $CDCl_3$): δ 7.64-7.61 (4 H, m), 7.48-7.44 (2 H, m), 7.40-7.38 (4 H, m), 7.26-7.24 (3 H, m), 6.89 (2 H, d, *J* = 8.6 Hz), 5.85 (1 H, ddd, *J* = 15.6, 6.1, 1.2 Hz), 5.72 (1 H, ddd, *J* = 15.6, 5.3, 0.8 Hz), 4.54-4.47 (3 H, m), 4.39-4.33 (1 H, m), 3.85 (1 H, dd, *J* = 10.4, 3.9 Hz), 3.81 (3 H, s), 3.74 (1 H, dd, *J* = 10.4, 3.9 Hz), 3.49 (1 H, dd, *J* = 9.6, 3.3 Hz), 3.31 (1 H, dd, *J* = 9.6, 8.3 Hz), 2.42 (1 H, br s), 1.07 (9 H, s).
^{13}C NMR (125 MHz, $CDCl_3$): δ 161.3, 159.5, 135.7, 135.6, 132.7, 132.6, 131.7, 130.2, 129.9, 129.6, 128.1, 128.0, 114.1, 92.9, 73.7, 73.2, 70.7, 65.3, 55.4, 54.1, 26.9, 19.4. ν_{max}/cm^{-1}: 3419, 3072, 2931, 2858, 1714, 1612, 1511, 1464, 1428, 1247, 1105, 819, 701. HRMS (ESI): $[M+Na]^+$ calculated for $C_{32}H_{38}Cl_3NO_5NaSi$: 672.1483; found: 672.1491.

$[\alpha]_D^{25°C}$ = - 4.6 (c 0.91 in $CHCl_3$).

ERETIC 2, general procedure

The samples were prepared according to the following method: 5 mg of sample were weight with a precision balance, then dissolved in 900 µL of deuterated chloroform. This solution was placed in a NMR tube (5 mm of diameter). Three types of samples were analysed: the starting material, the evaporated crude mixture and the purified product. Residual remaining solvents and side-reagents have been considered for different calculations.

For each sample, the ^{1}H NMR spectra were recorded at 298K on a Bruker Avance III 600 MHz equipped with a TCI cryoprobe (5 mm of diameter) cooled down with helium. Each experiment was recorded using a quantitative method. The longitudinal relaxation time (T1) was evaluated to fix the relaxation delay (D1 = 25 seconds) and the pulse (P1 = 8.15 µseconds).

After recording of spectra, the ERETIC 2 method's Topsin 3.2 pl 6 software was used to evaluate the crude composition.

NMR spectra

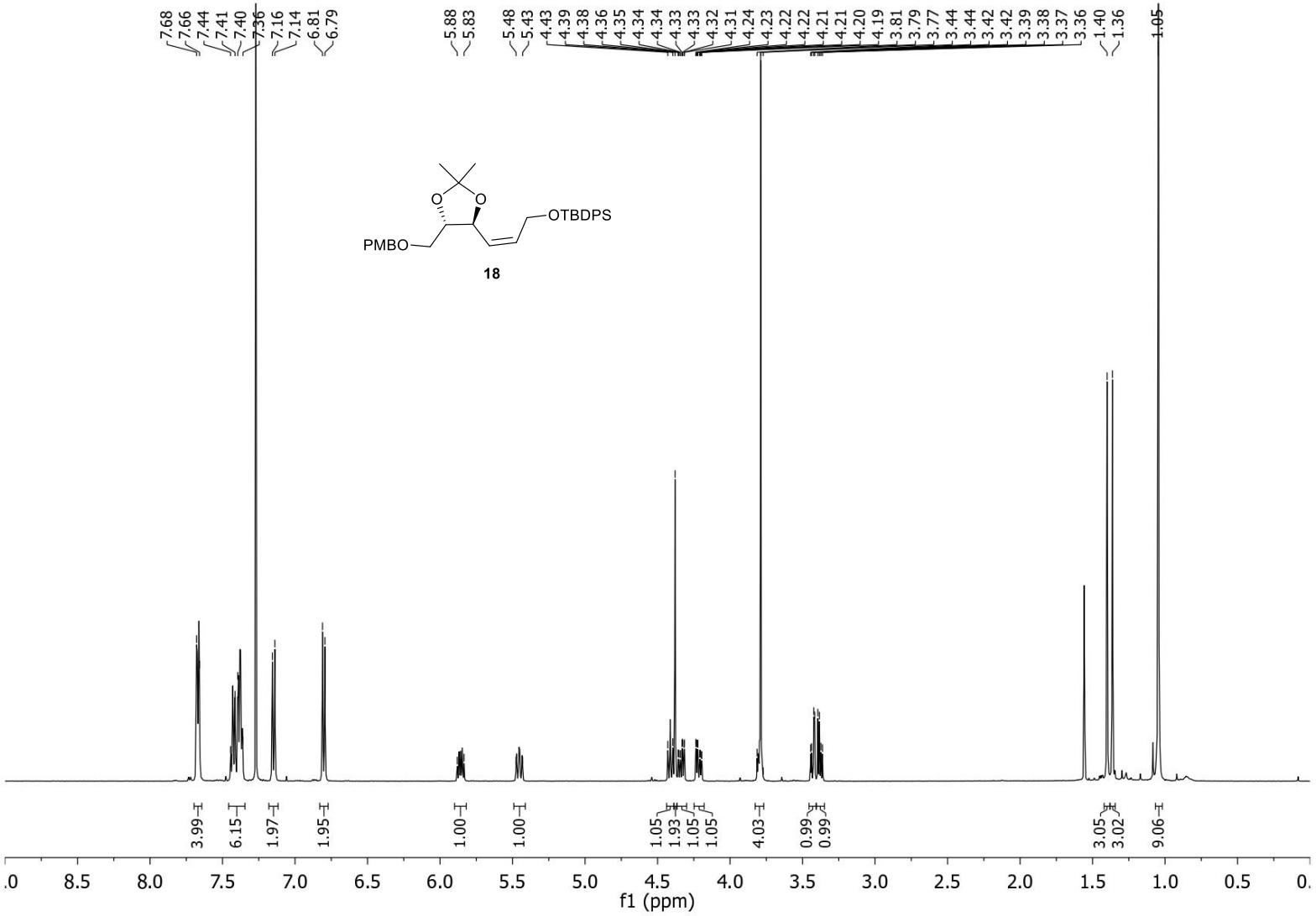

Figure S7: ^{1}H NMR spectrum of 18 (500 MHz, $CDCl_3$).

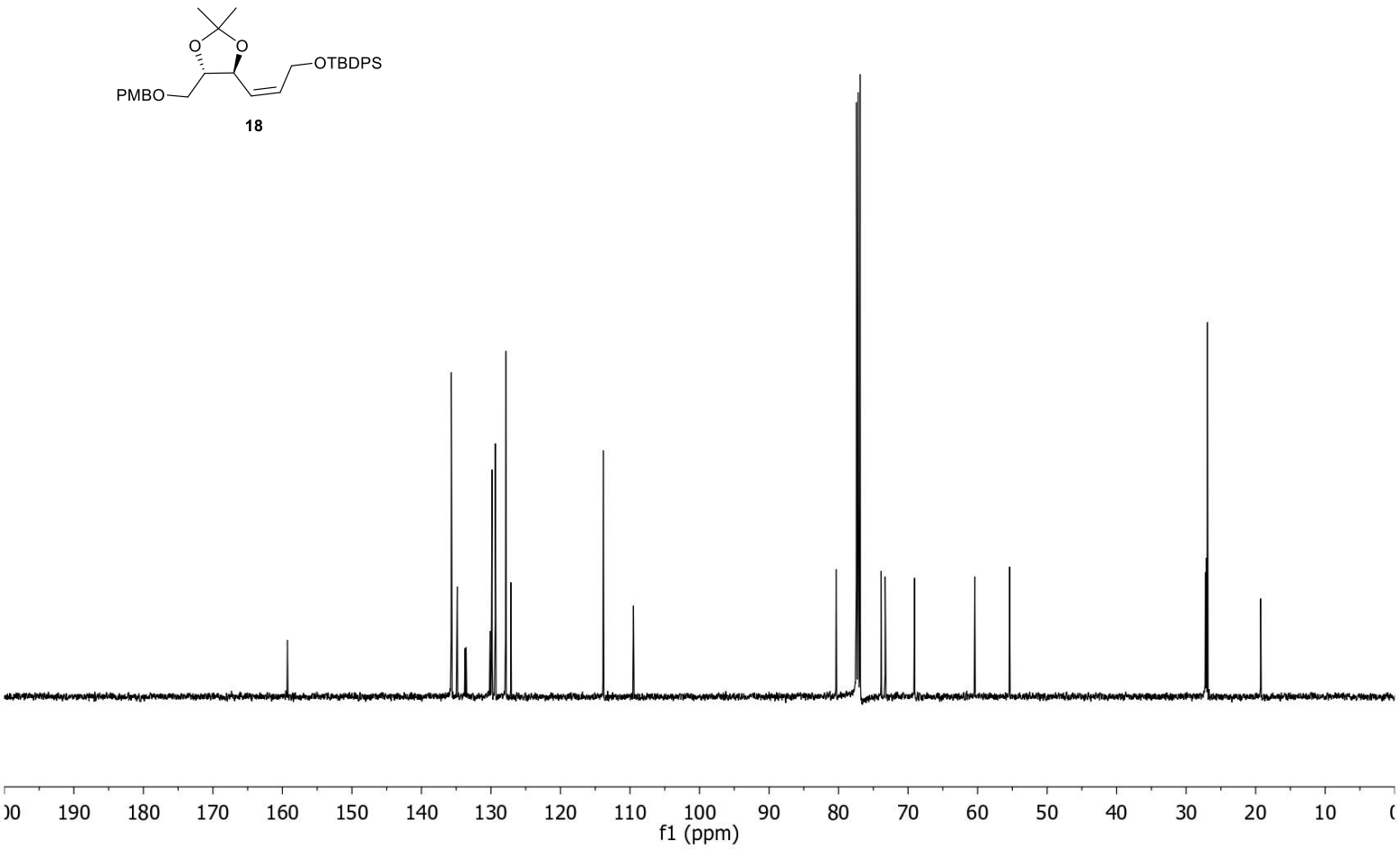

Figure S8: ^{13}C NMR spectrum of 18 (125 MHz, $CDCl_3$).

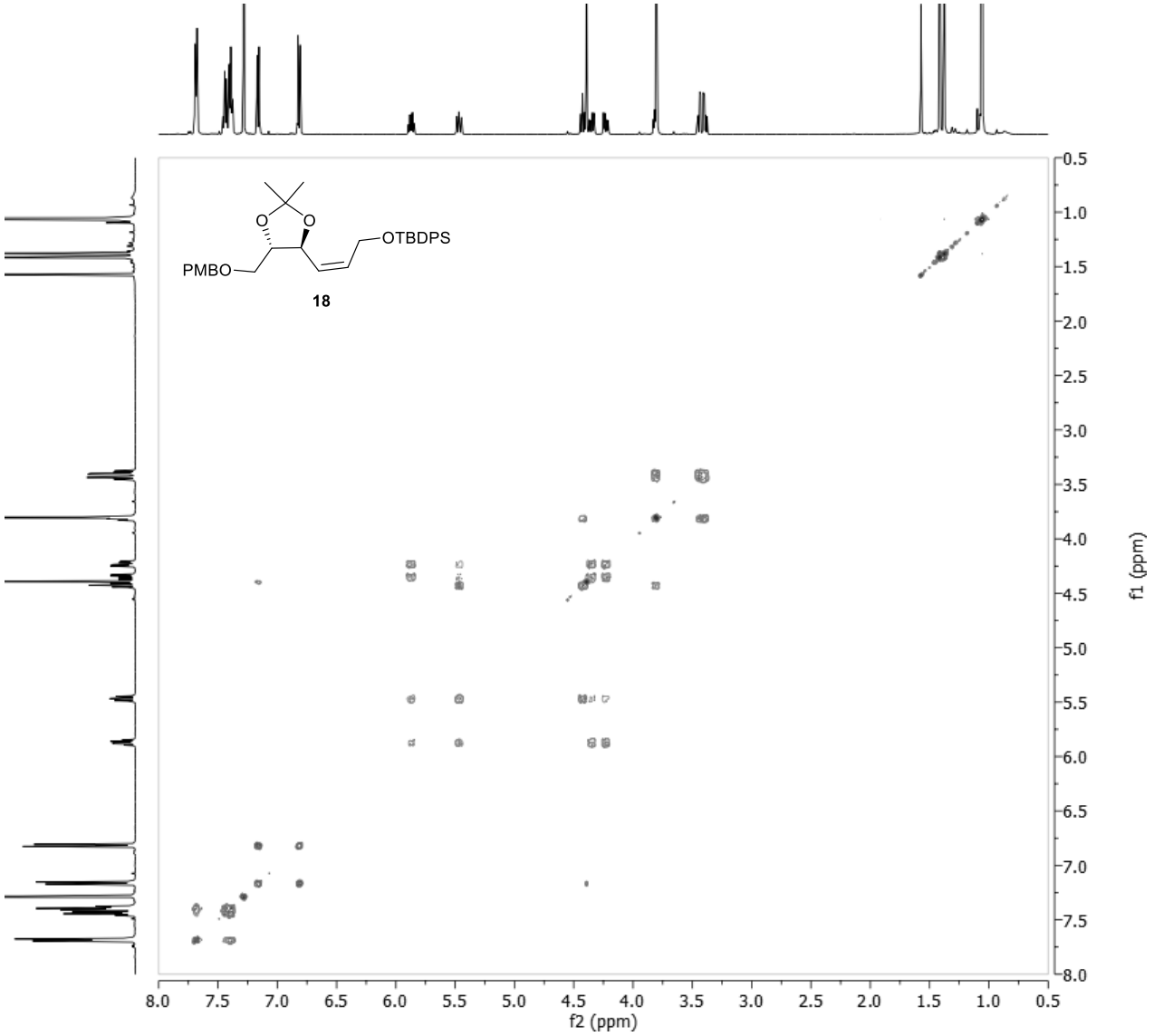

Figure S9: COSY spectrum of 18 (500 MHz, $CDCl_3$).

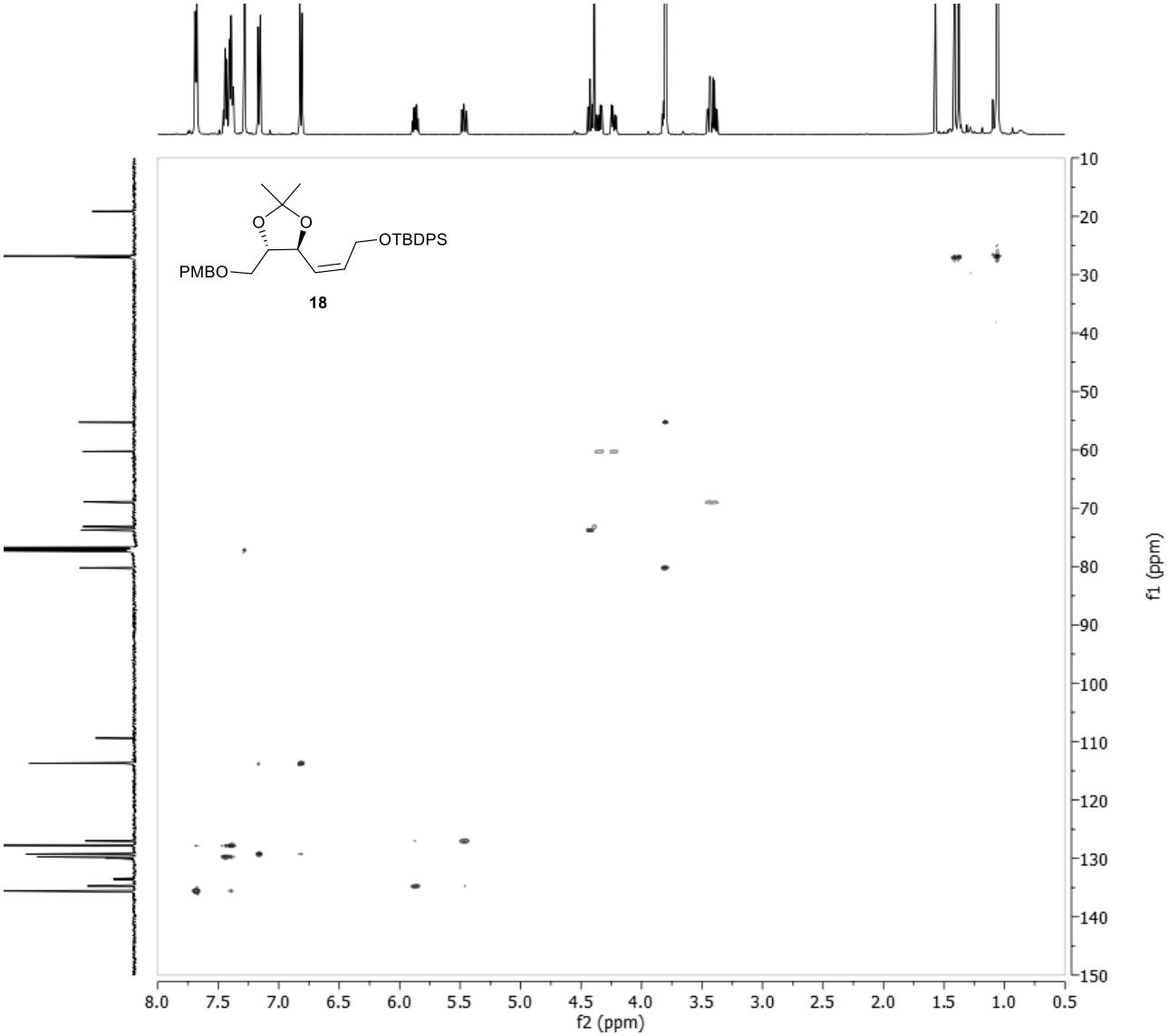

Figure S10: HSQC spectrum of 18 (500 MHz, $CDCl_3$).

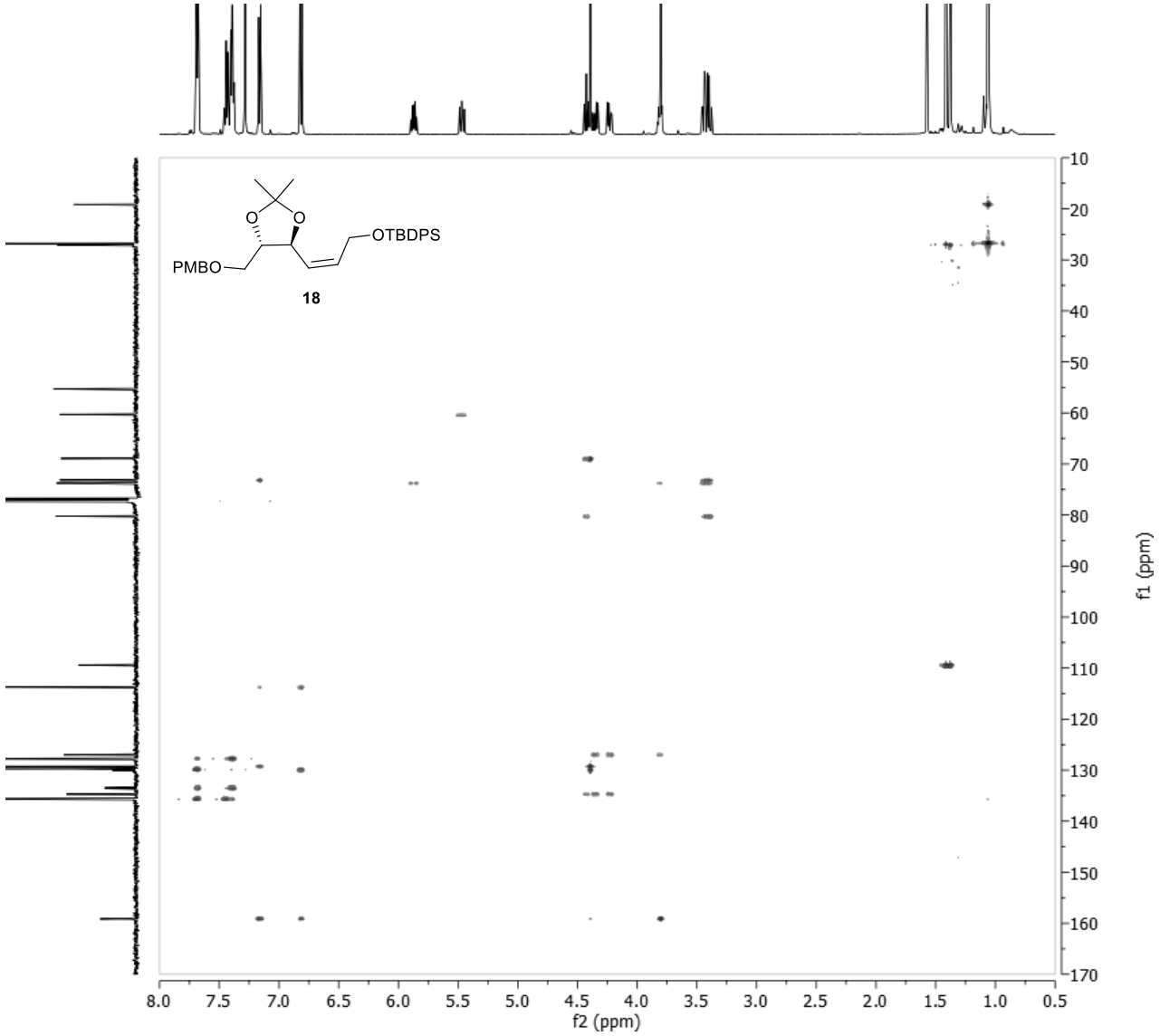

Figure S11: HMBC spectrum of 18 (500 MHz, $CDCl_3$).

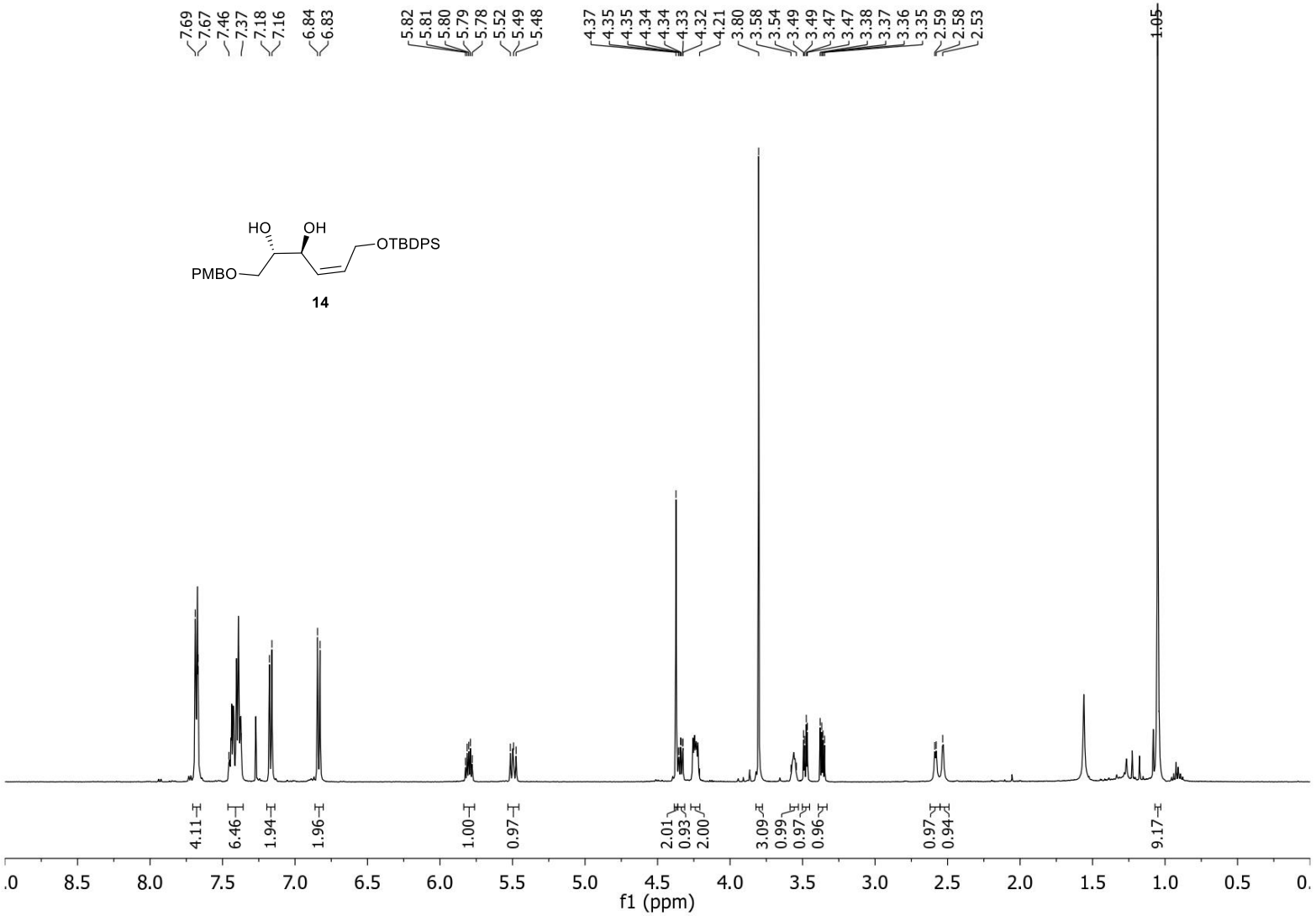

Figure S12: ^{1}H NMR spectrum of 14 (500 MHz, $CDCl_3$).

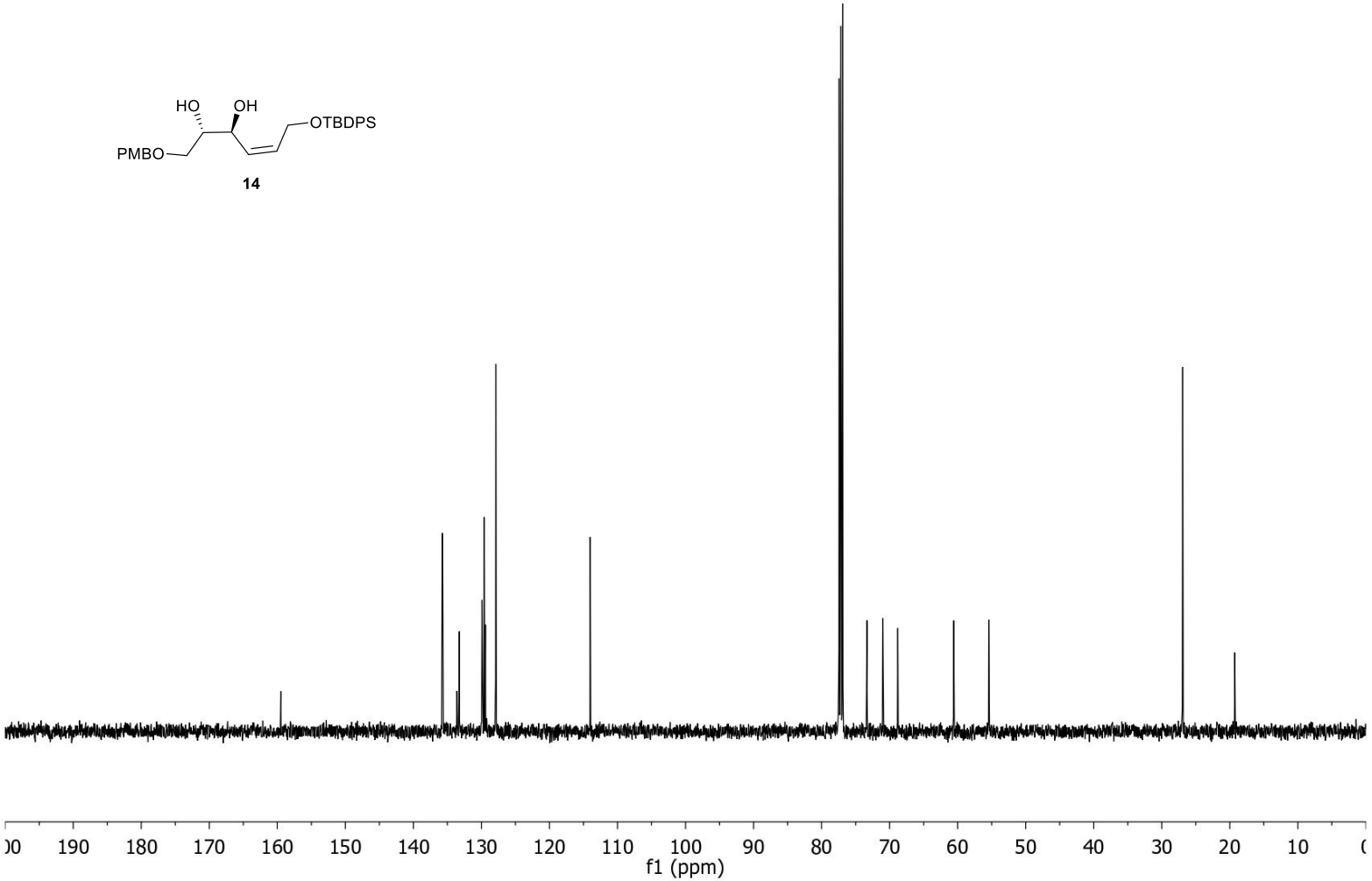

Figure S13: ^{13}C NMR spectrum of 14 (125 MHz, $CDCl_3$).

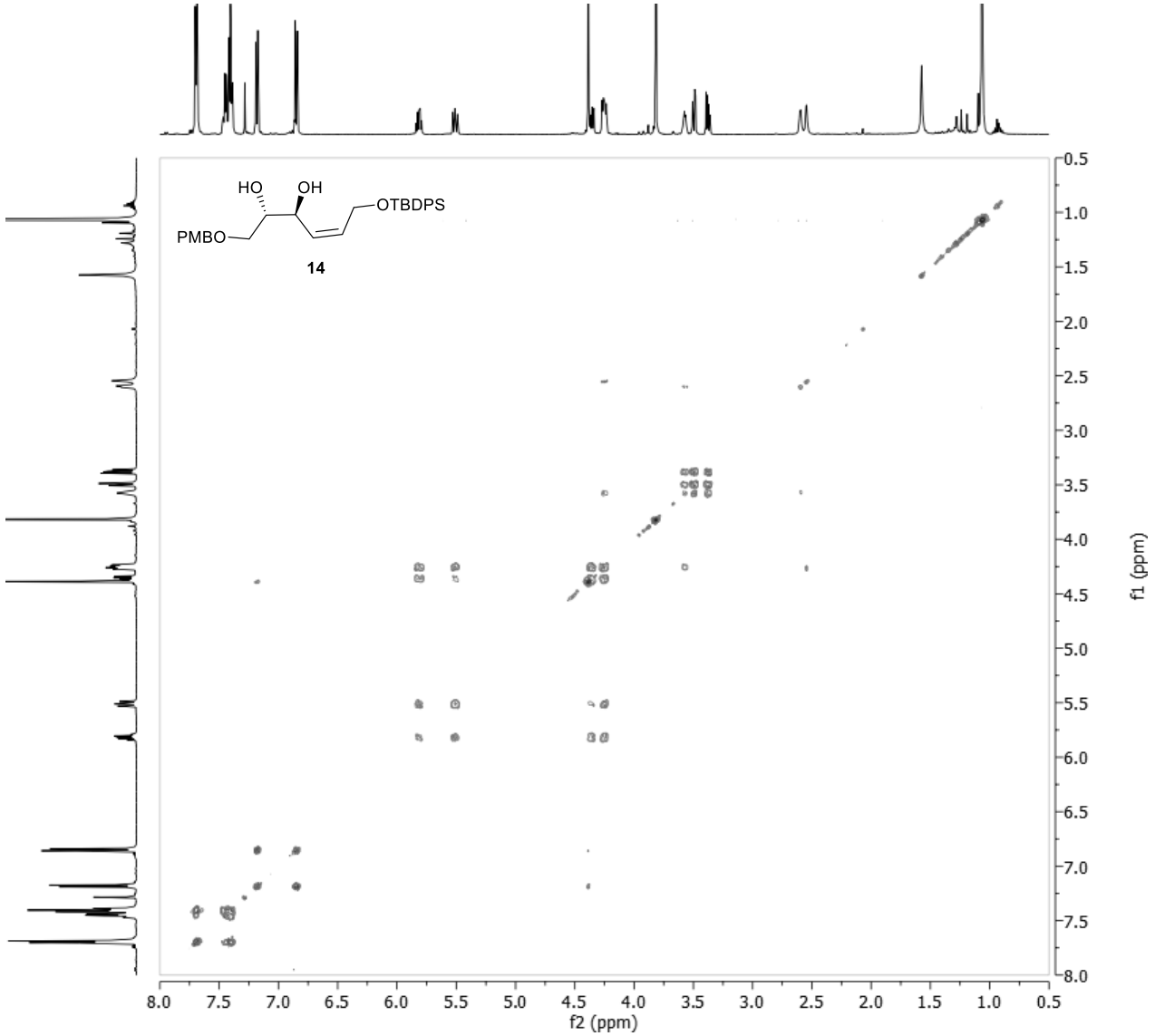

Figure S14: COSY spectrum of 14 (500 MHz, $CDCl_3$).

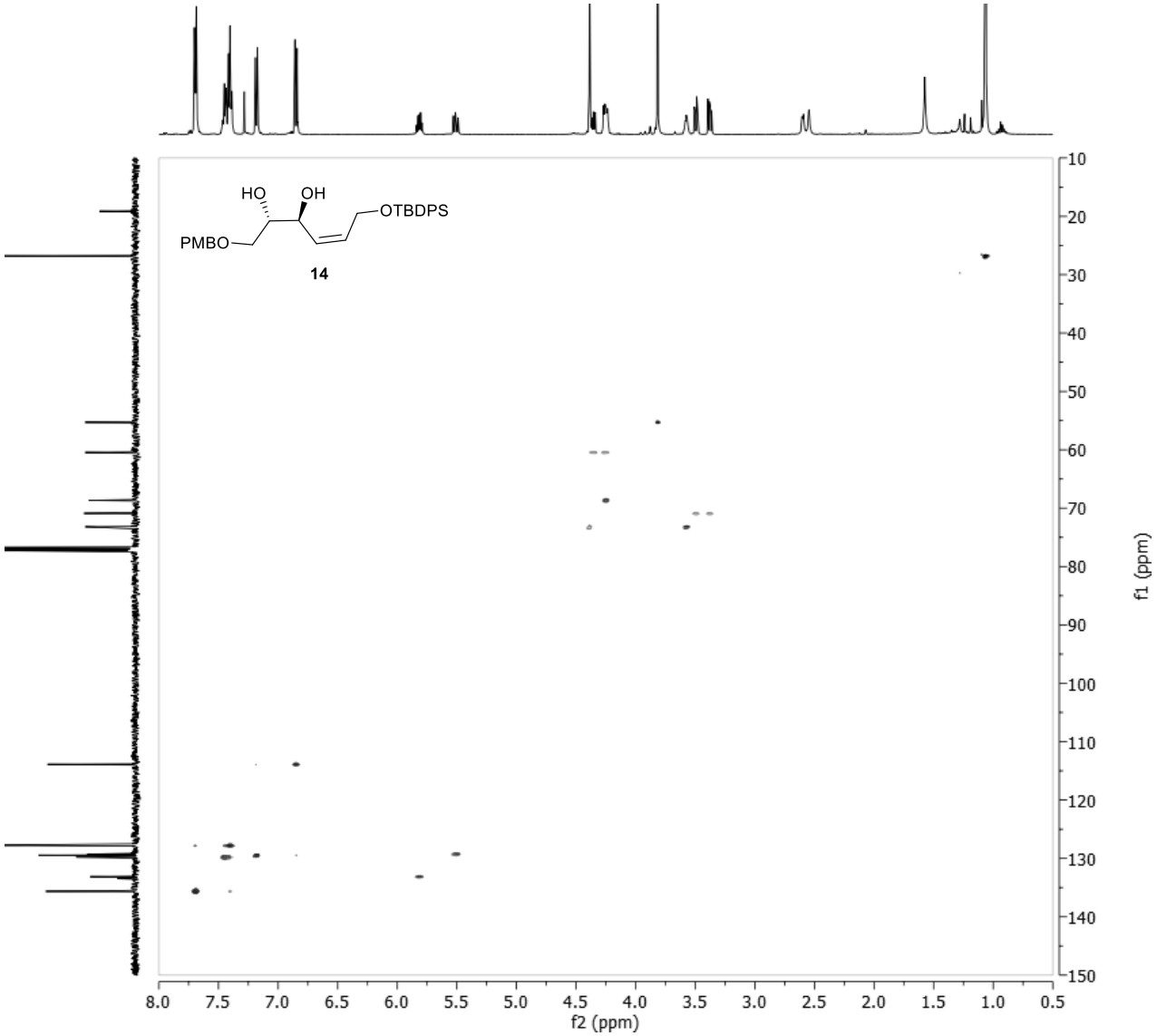

Figure S15: HSQC spectrum of 14 (500 MHz, $CDCl_3$).

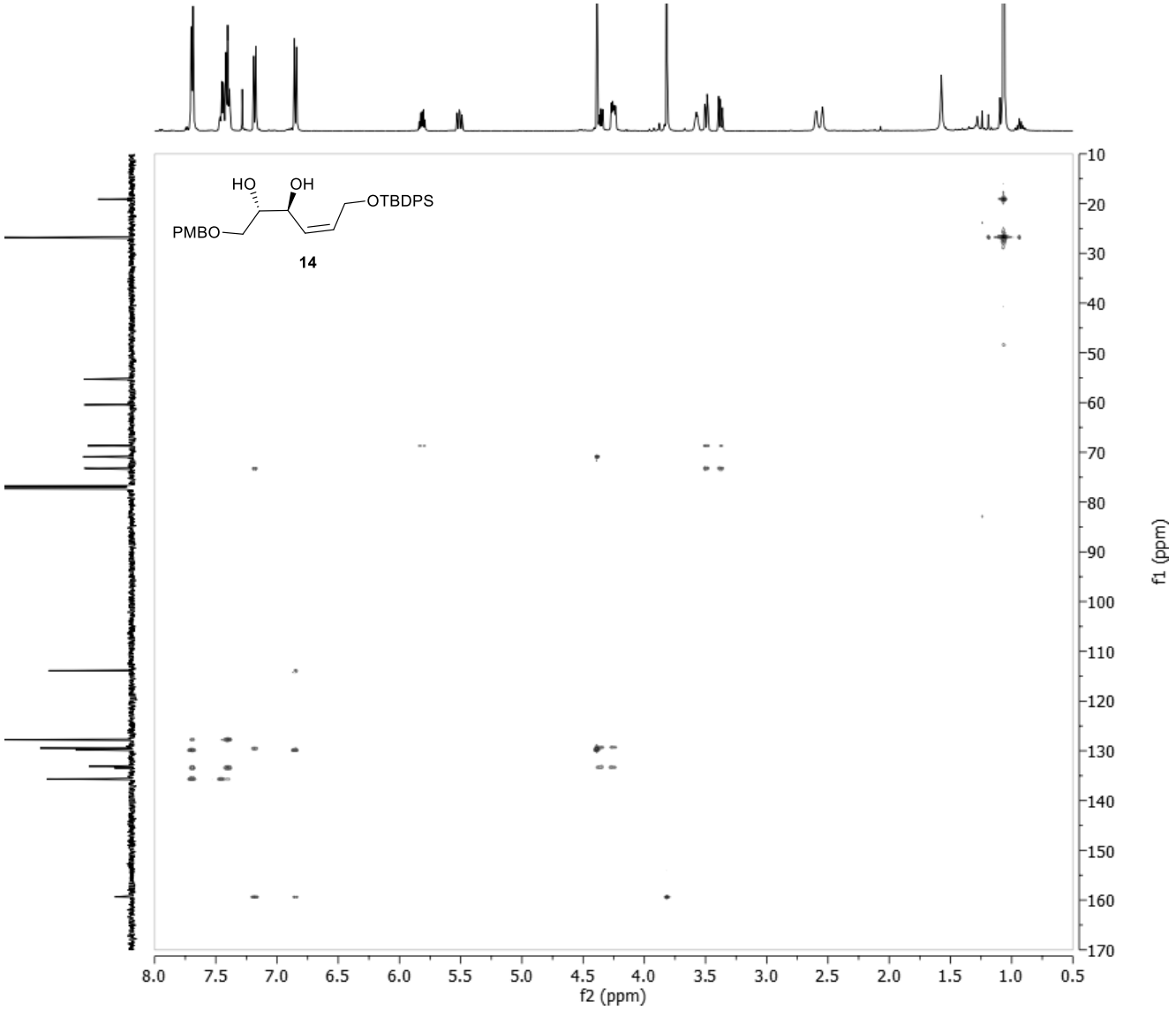

Figure S16: HMBC spectrum of 14 (500 MHz, $CDCl_3$).

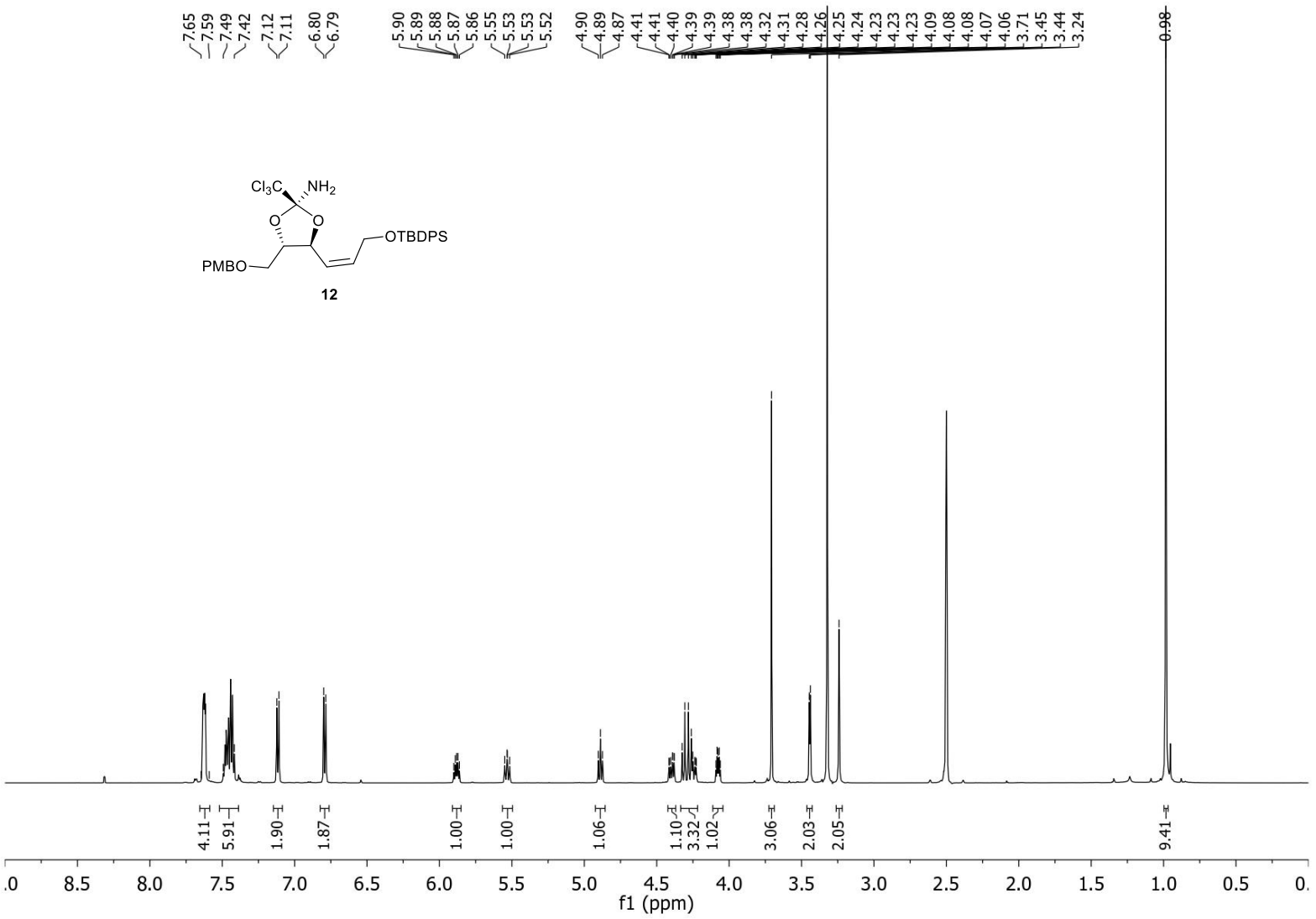

Figure S17: ^{1}H NMR spectrum of 12 (less polar) (600 MHz, DMSO-d_6).

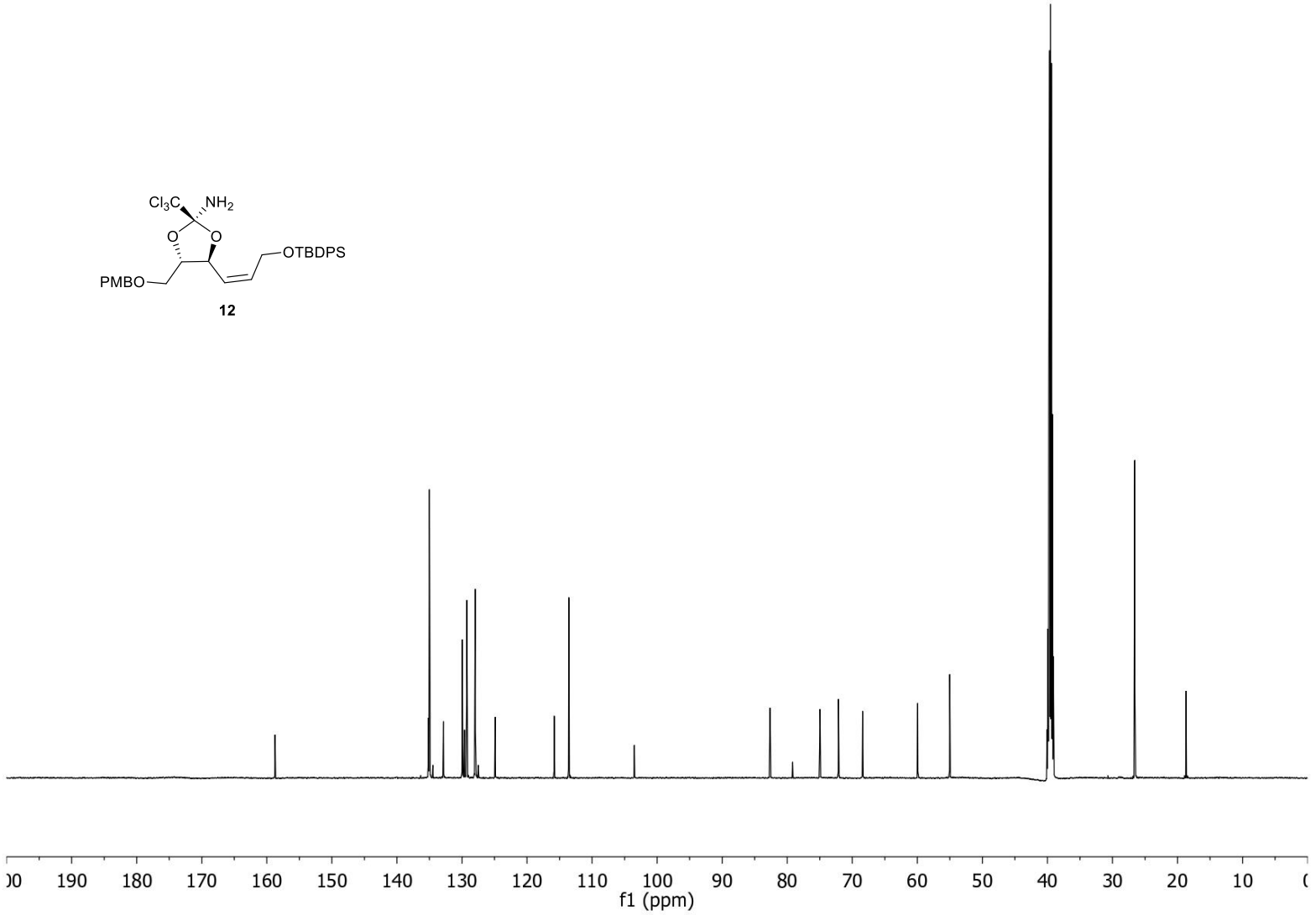

Figure S18: ^{13}C NMR spectrum of 12 (less polar) (150 MHz, DMSO-d_6).

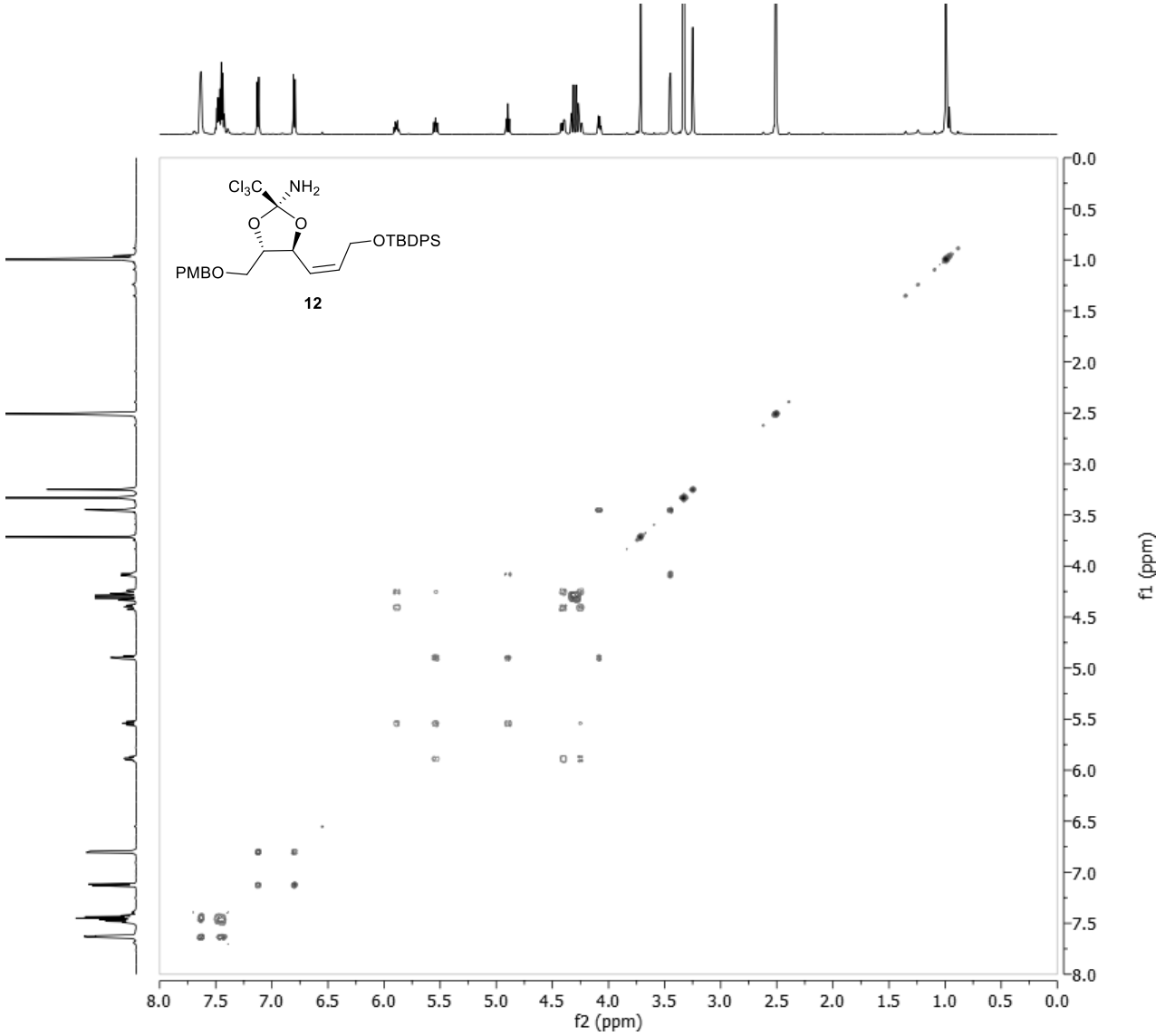

Figure S19: COSY spectrum of 12 (less polar) (600 MHz, DMSO-d_6).

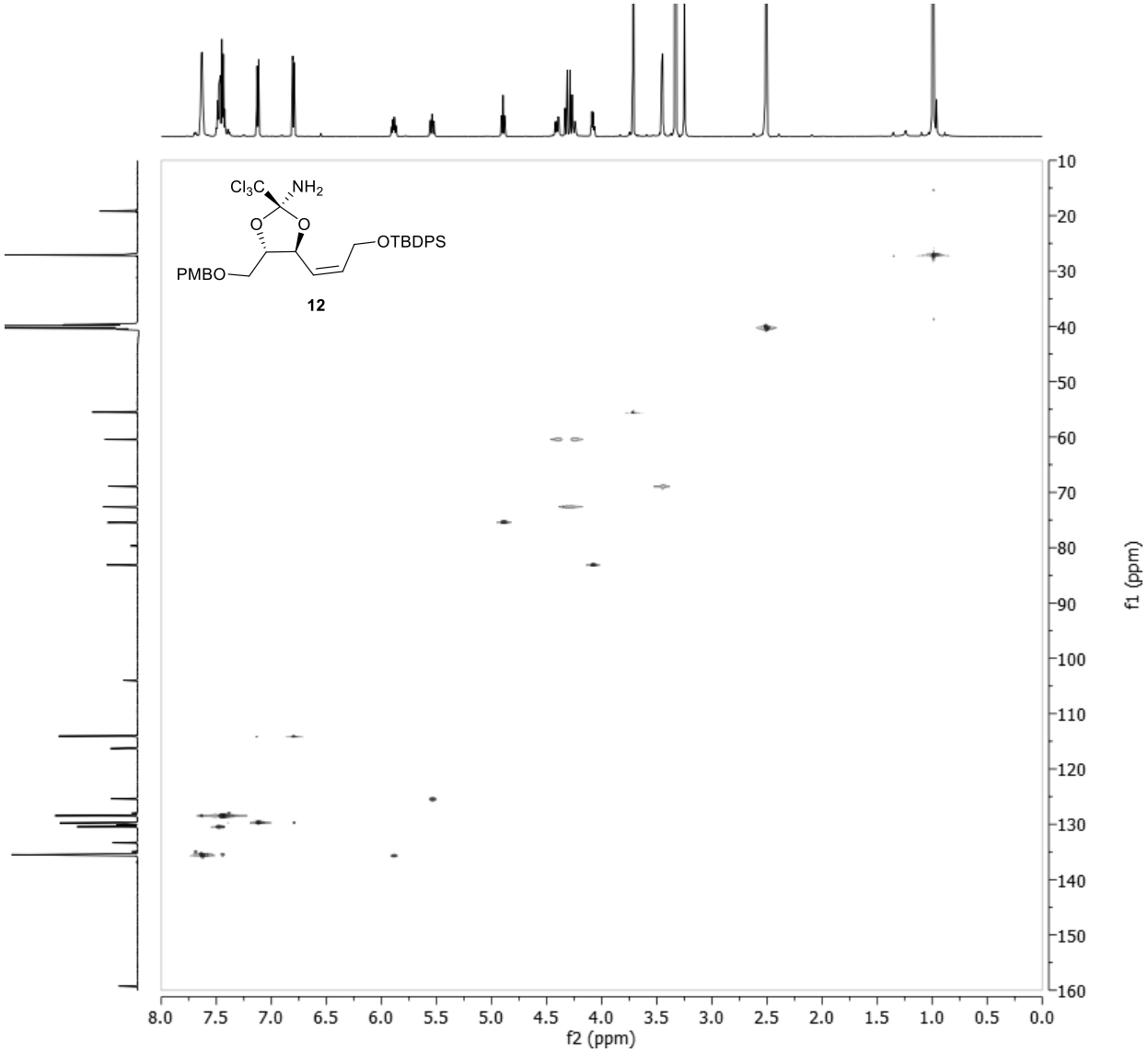

Figure S20: HSQC spectrum of 12 (less polar) (600 MHz, DMSO-d_6).

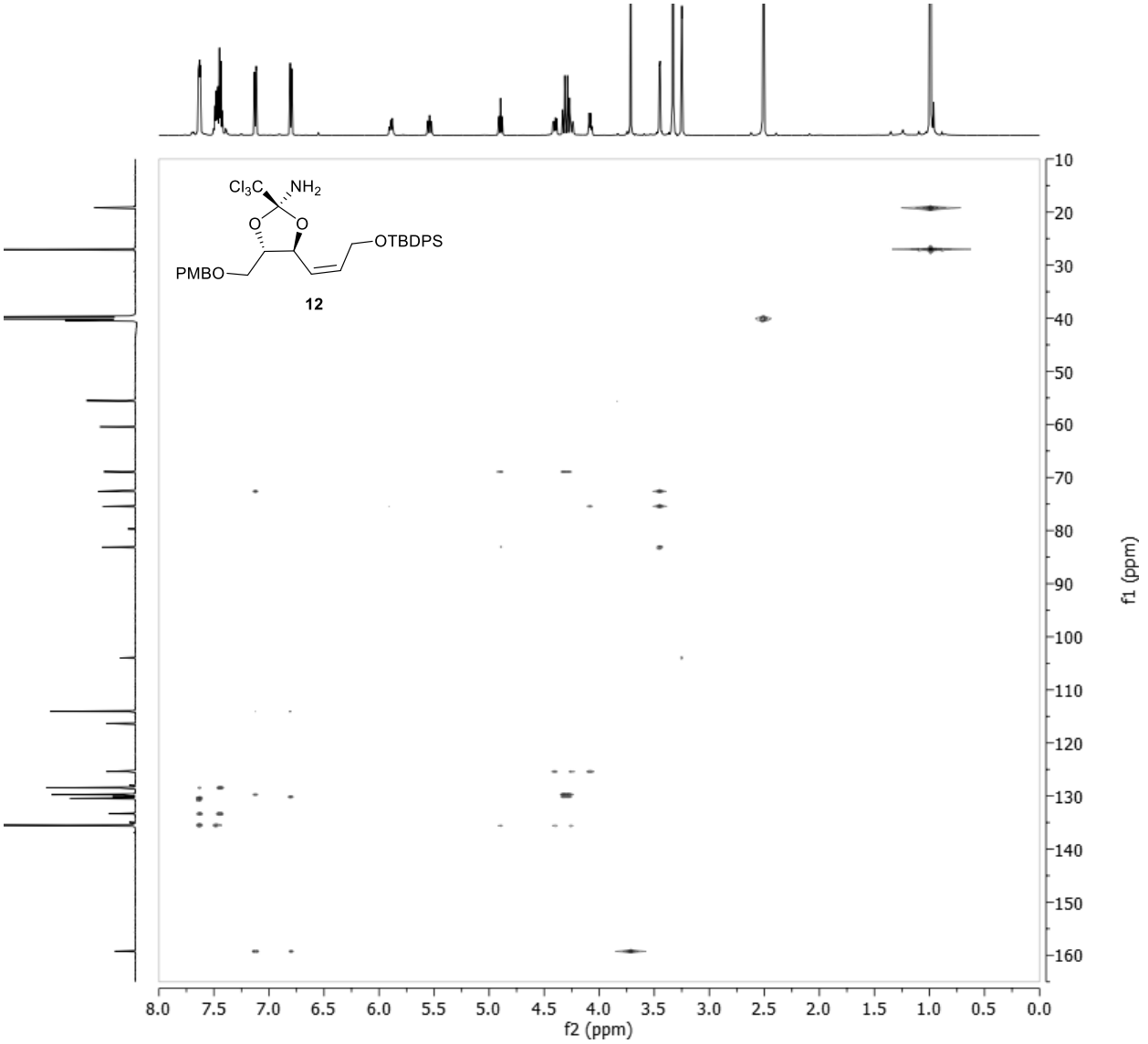

Figure S21: HMBC spectrum of 12 (less polar) (600 MHz, DMSO-d_6).

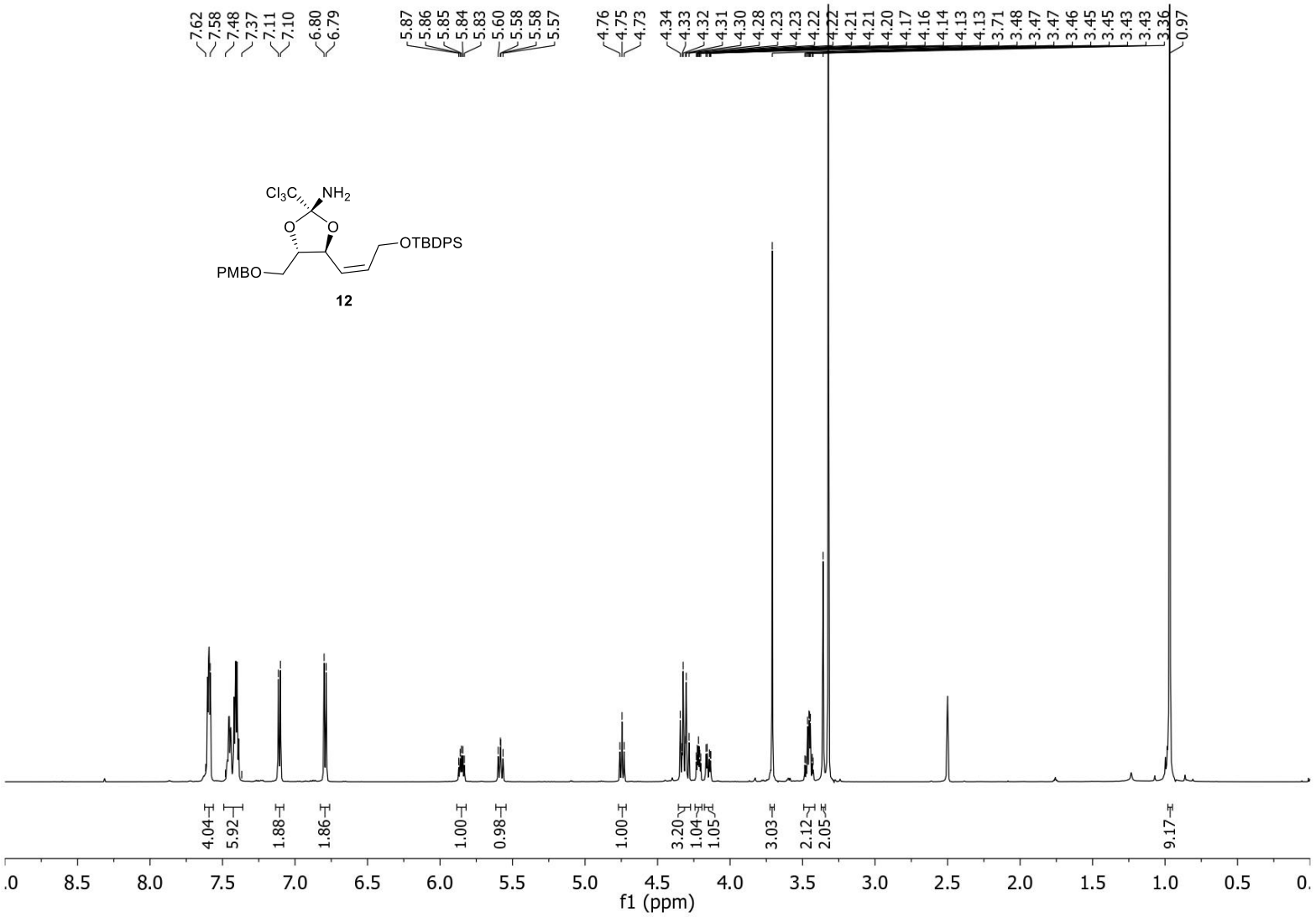

Figure S22: ^{1}H NMR spectrum of 12 (polar) (600 MHz, DMSO-d_6).

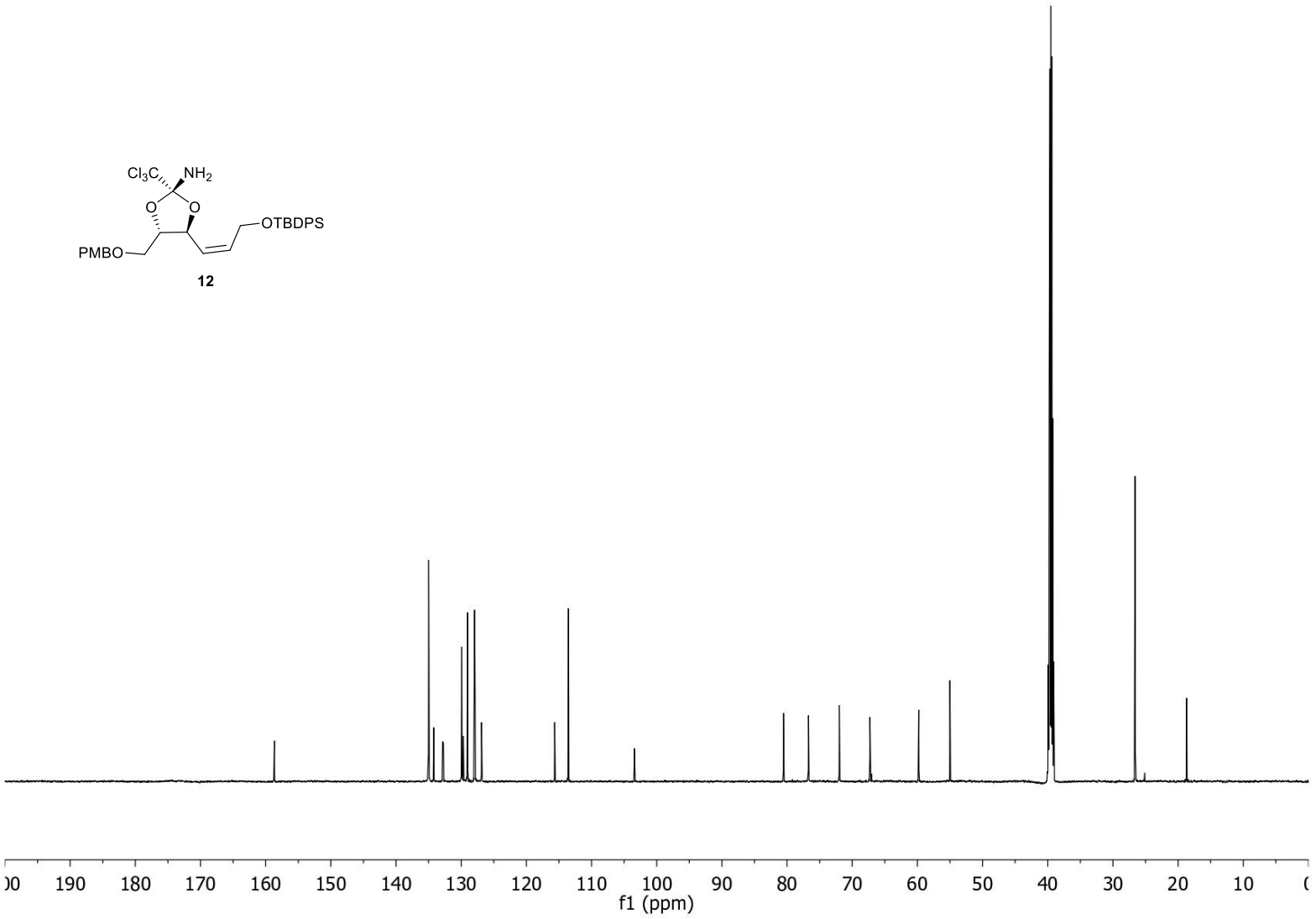

Figure S23: ^{13}C NMR spectrum of 12 (polar) (150 MHz, DMSO-d_6).

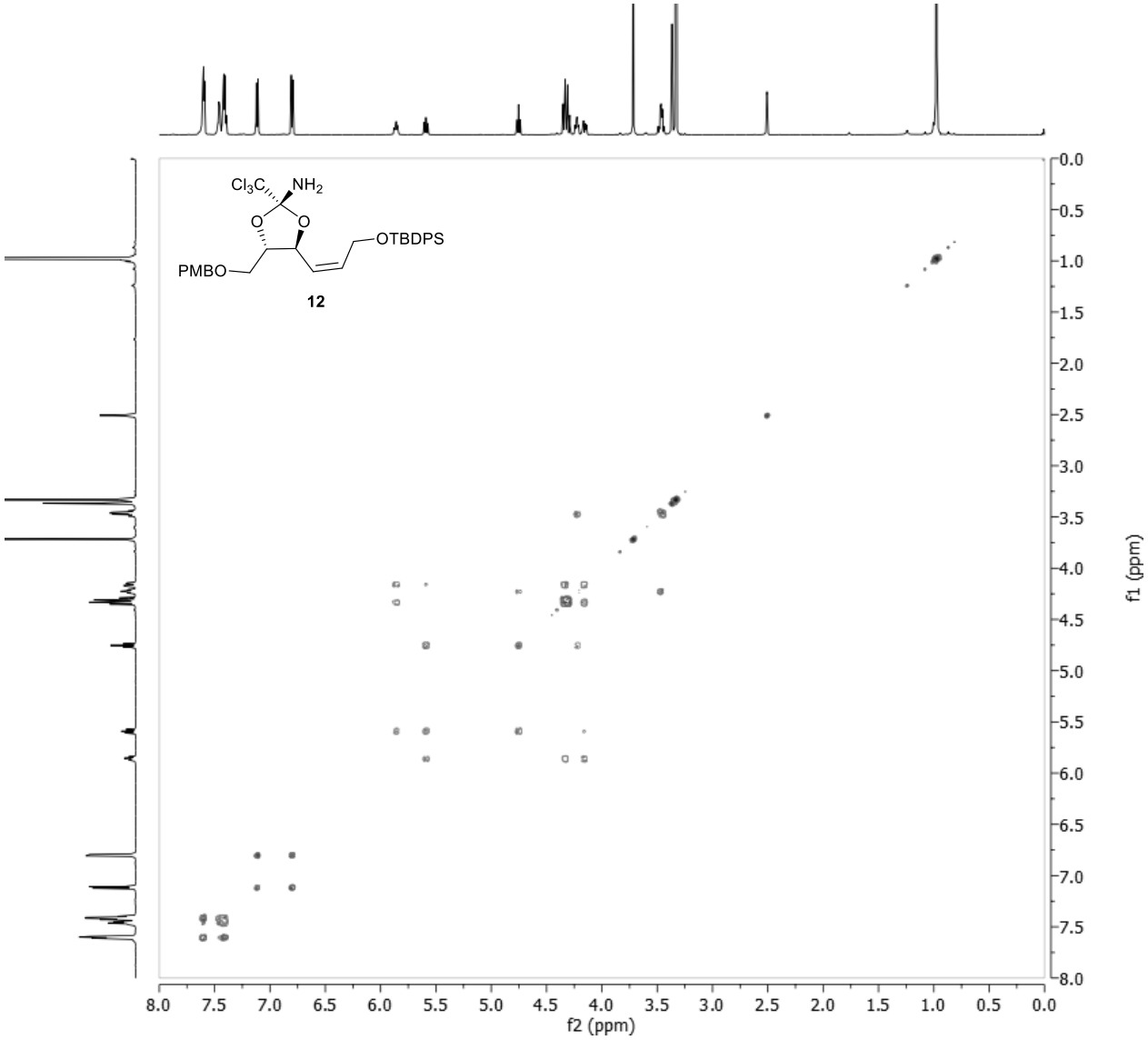

Figure S24: COSY spectrum of 12 (polar) (600 MHz, DMSO-d_6).

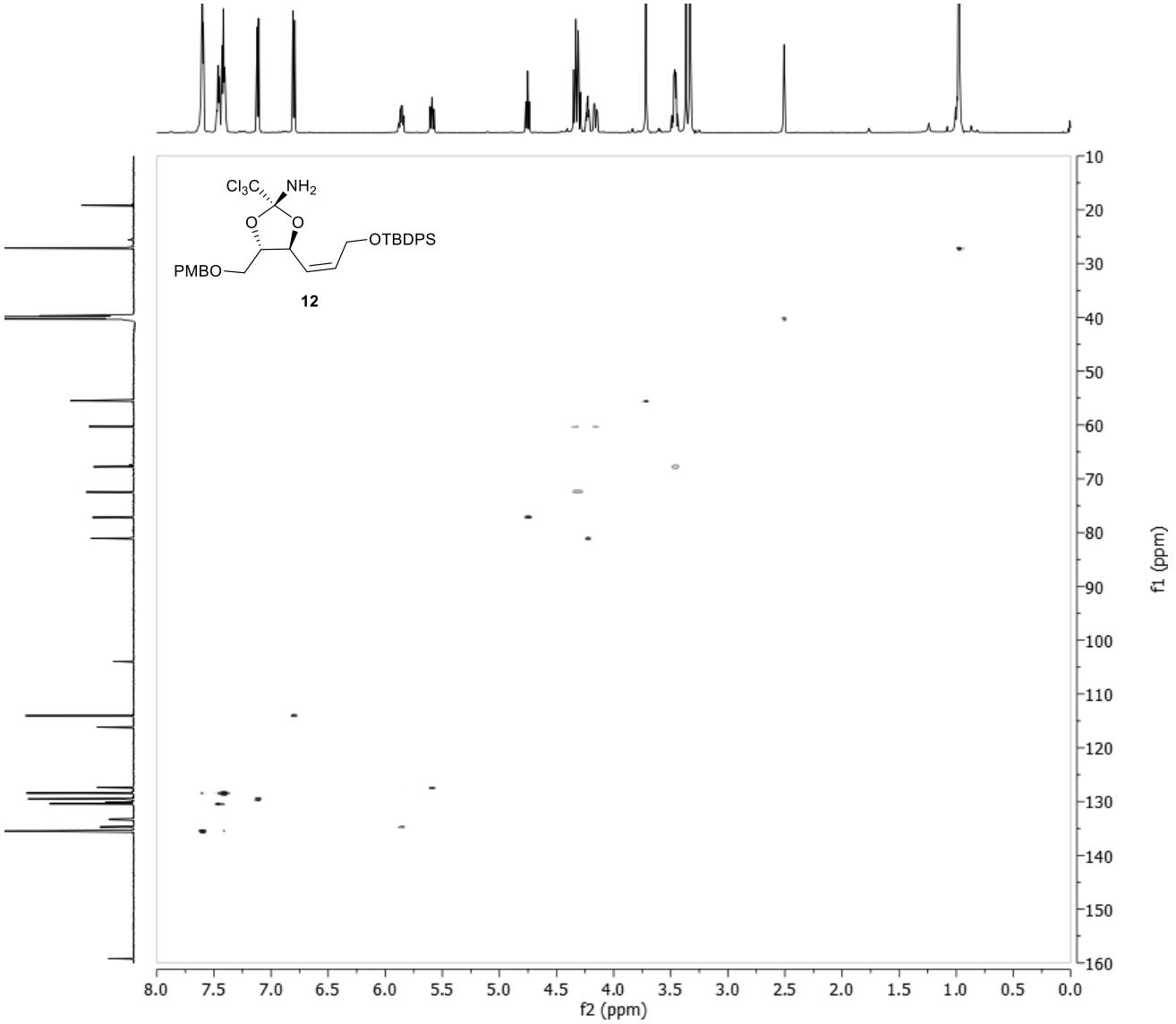

Figure S25: HSQC spectrum of 12 (polar) (600 MHz, DMSO-d_6).

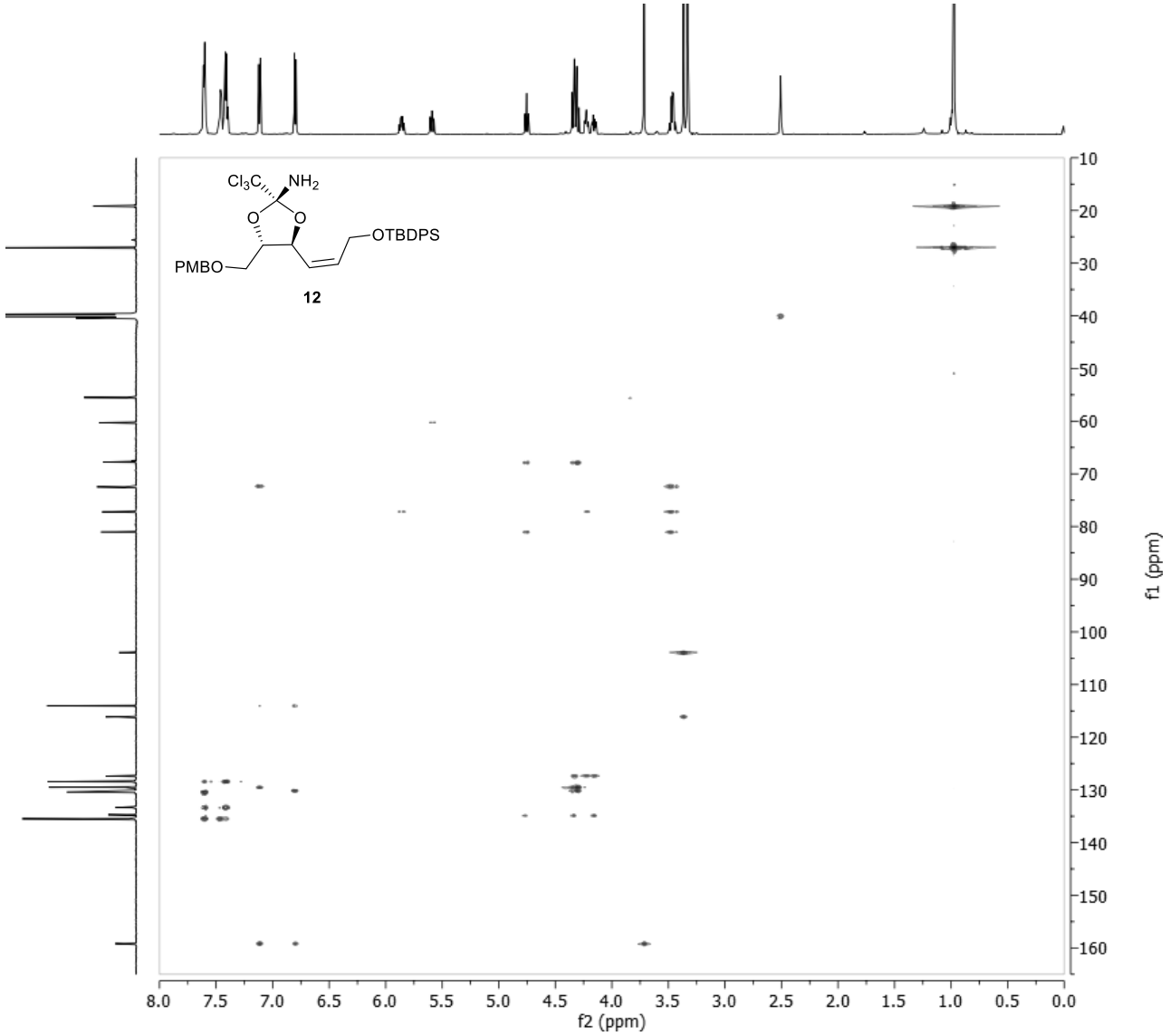

Figure S26: HMBC spectrum of 12 (polar) (600 MHz, DMSO-d_6).

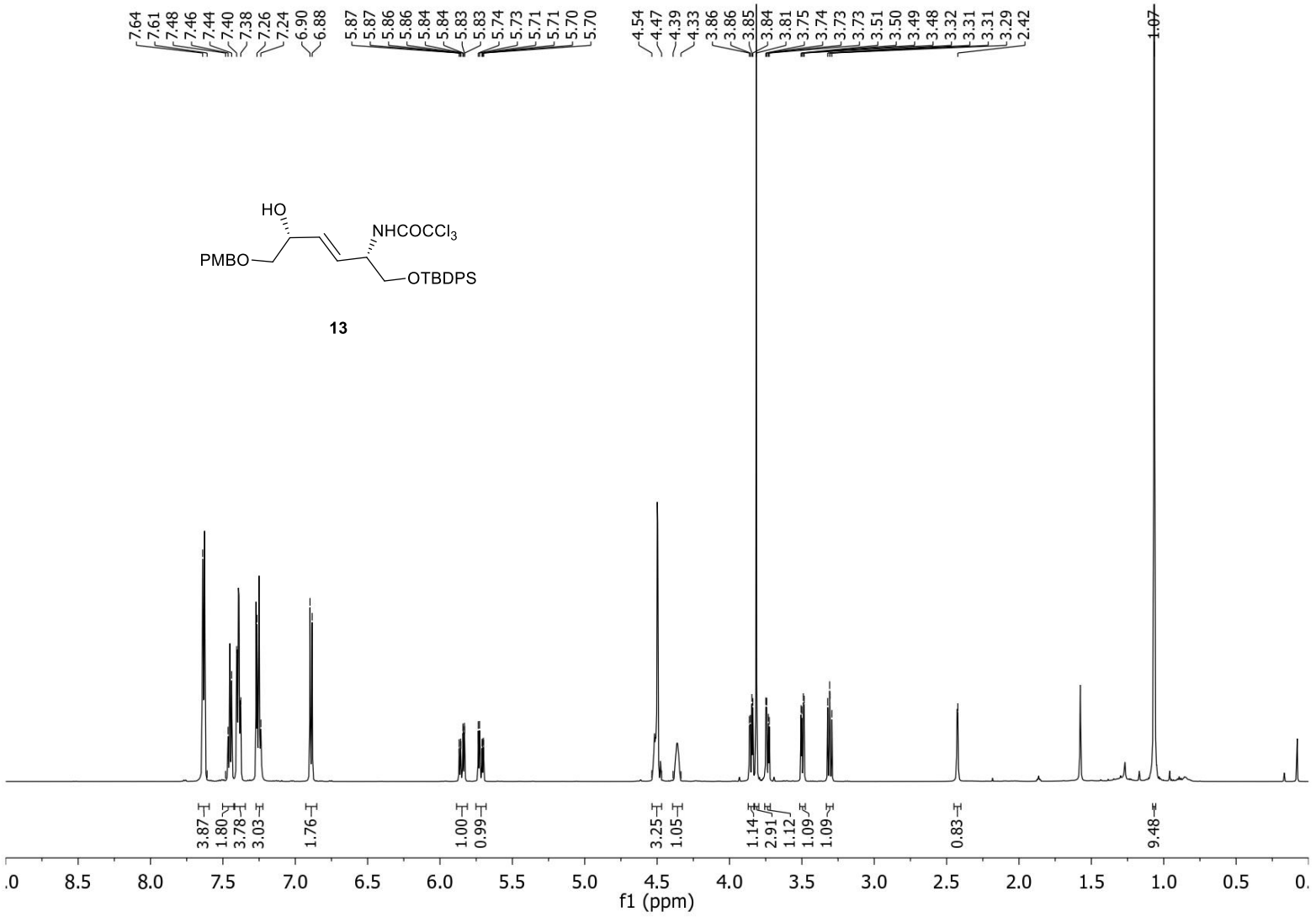

Figure S27: ^{1}H NMR spectrum of 13 (600 MHz, $CDCl_3$).

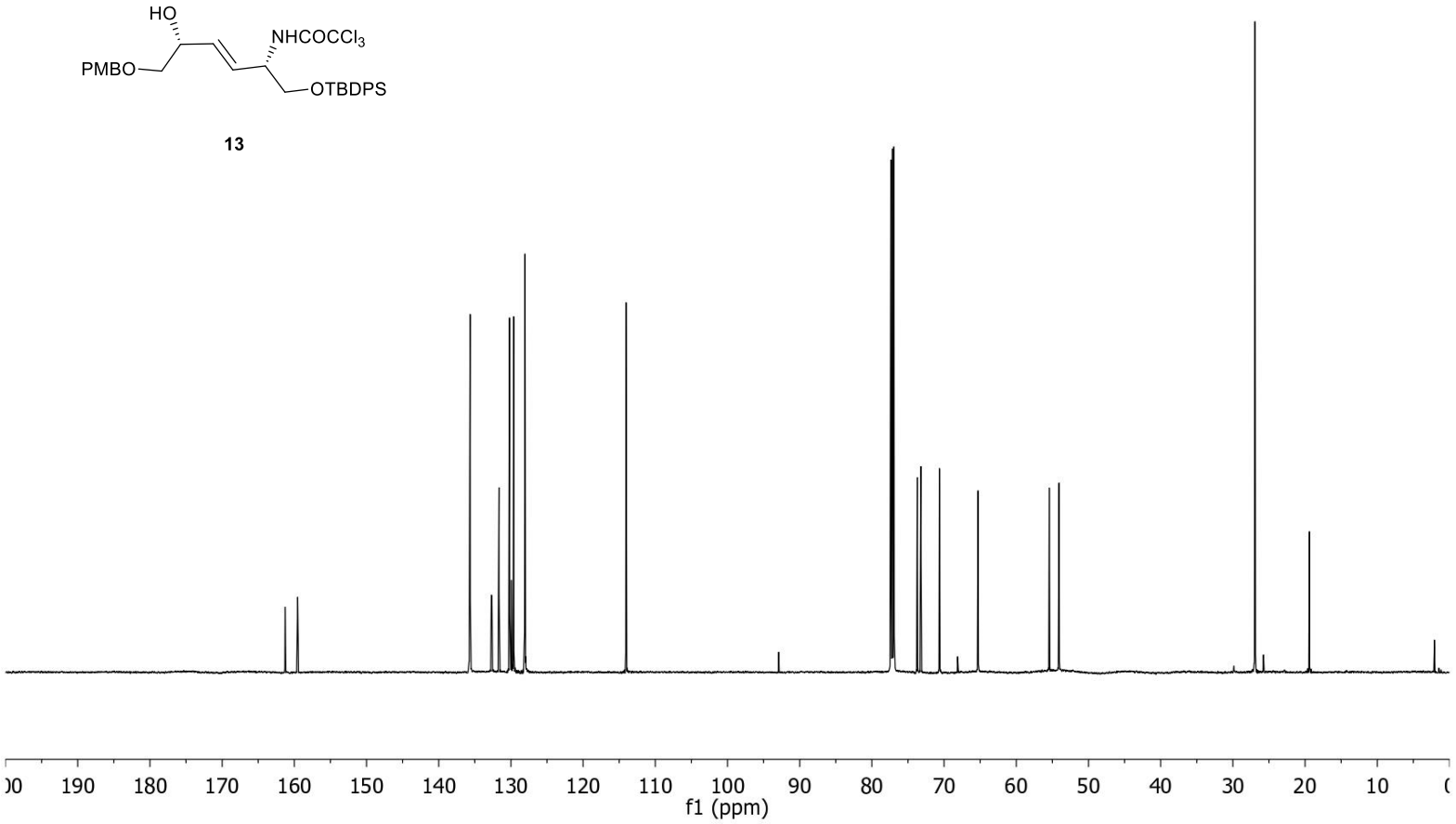

Figure S28: ^{13}C NMR spectrum of 13 (150 MHz, $CDCl_3$).

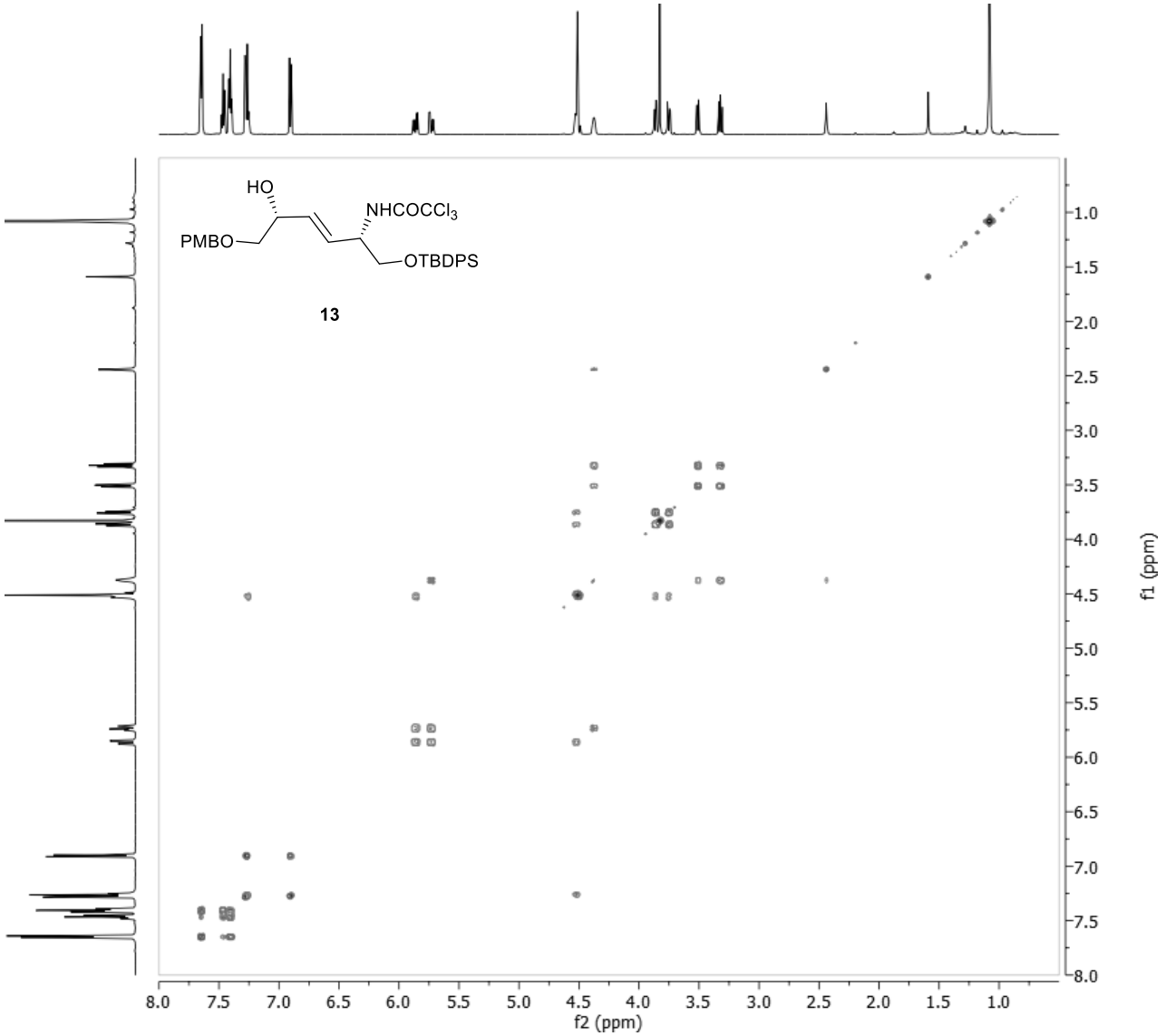

Figure S29: COSY spectrum of 13 (600 MHz, $CDCl_3$).

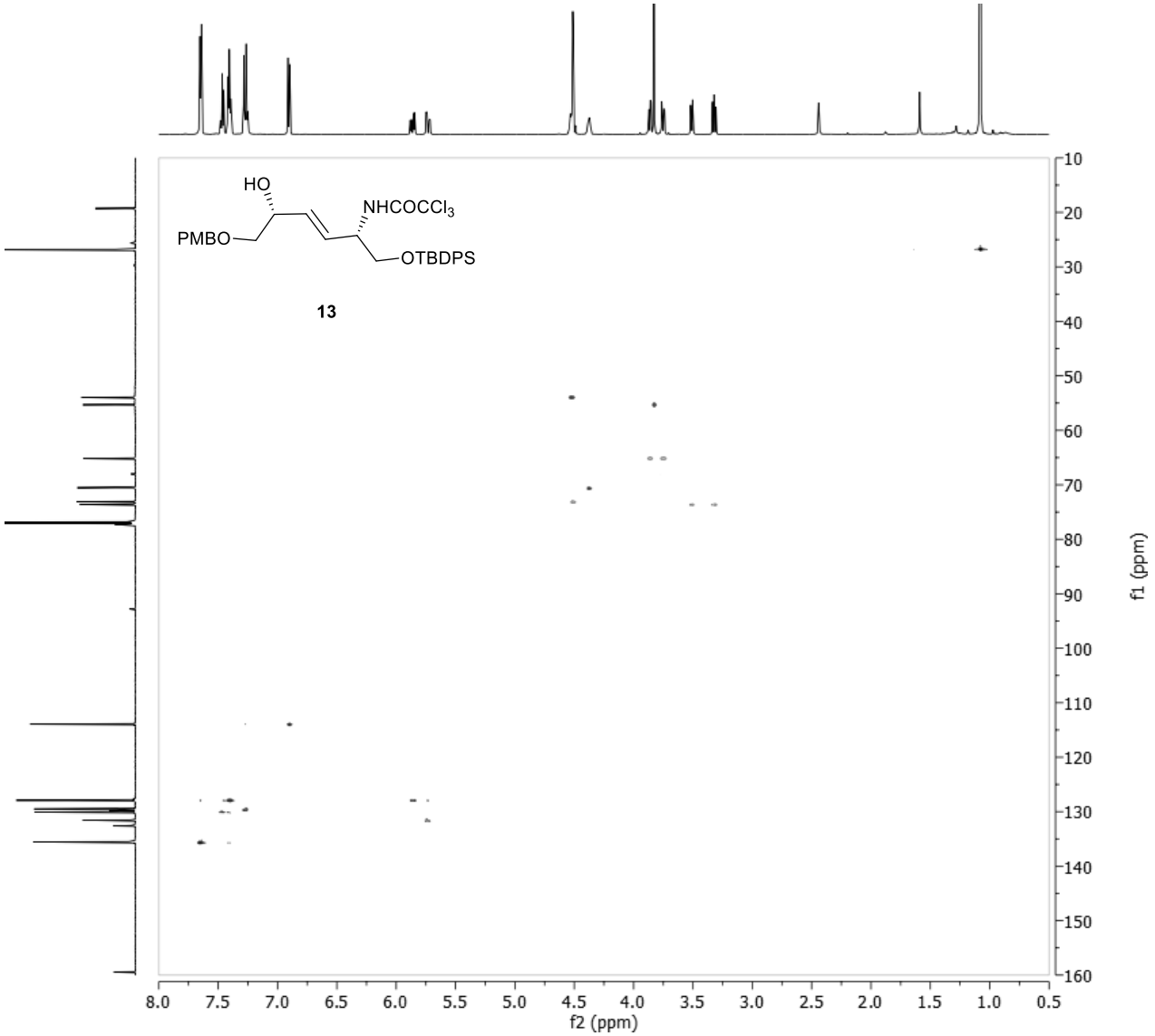

Figure S30: HSQC spectrum of 13 (600 MHz, $CDCl_3$).

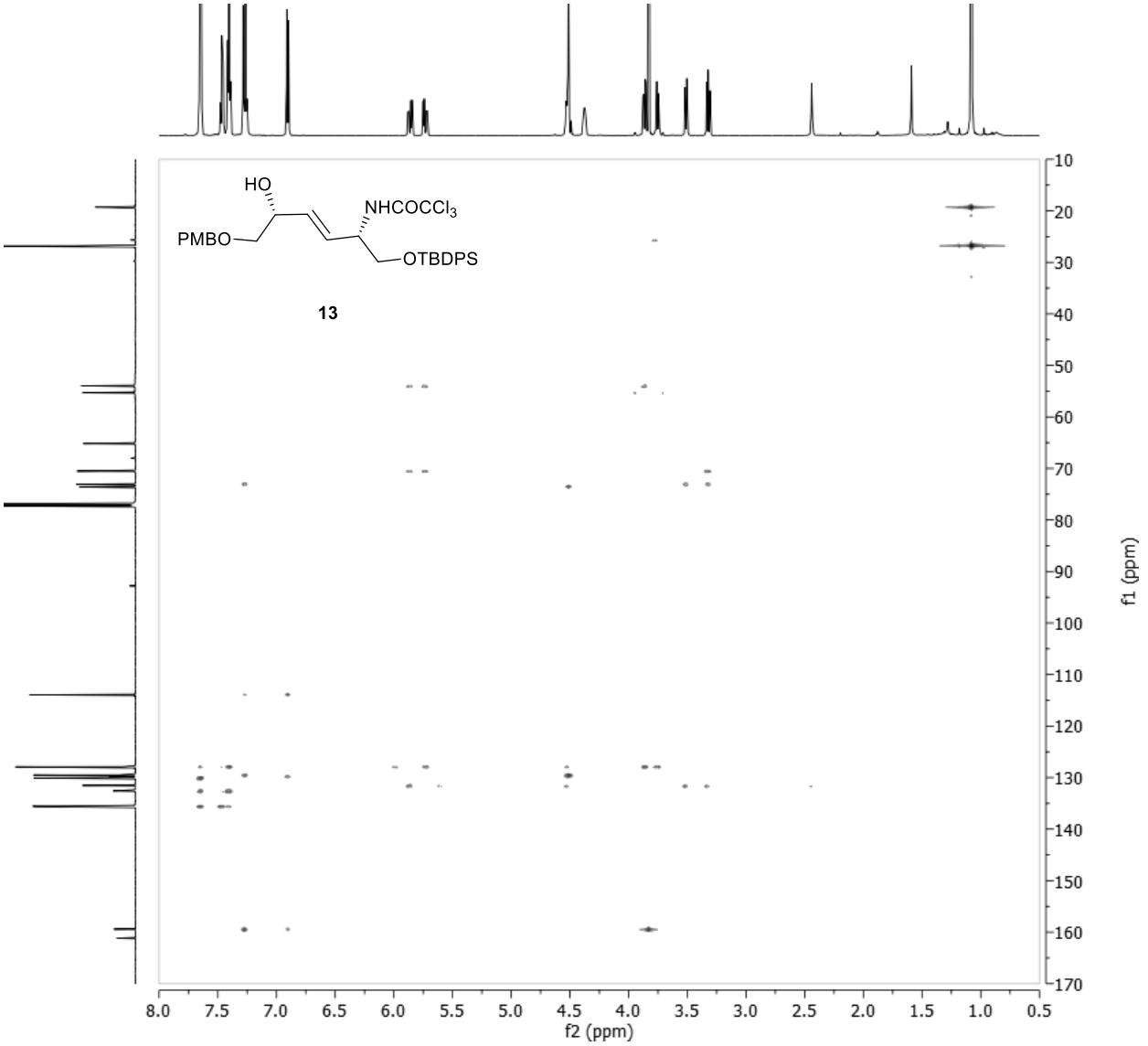

Figure S31: HMBC spectrum of 13 (600 MHz, $CDCl_3$).

Theoretical part

The Overman reaction is a process involving several transformations (Fig. 1), with all species in equilibrium, each entity existing as many conformers. The hypothesis of our work relies on the supposition that some stable species have the disadvantage not to lead to the desired Overman transformation, which would explain the difficulty of this process.

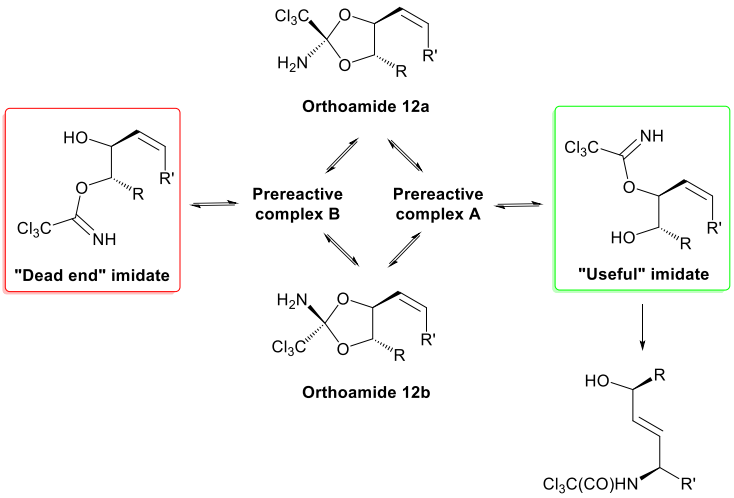

Figure 1 Species and transformations in the Overman process.

Before going deeper into studies of transitions states, it is useful to give a general Gibbs free energy figure in order to define the different described entities, i.e. orthoamides, prereactive complexes, transition states and imidates (Fig. 2).

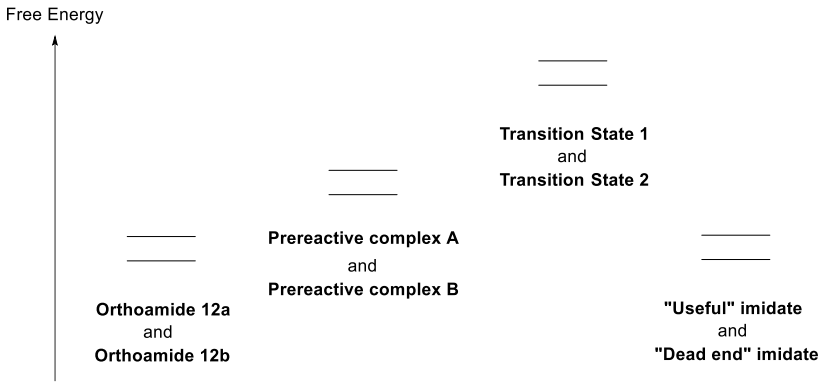

Figure 2 General free energy figure with all the species.

A) Computation studies on the different conformers of orthoamides **12a** and **12b**

First of all, it is important to precise that the two diastereoisomeric orthoamides **12a** (*R*) and **12b** (S), when separated by column chromatography on silica gel, interconvert on standing in solution in $CDCl_3$. Firstly, the study of major staggered conformers (around the C-N bond) of the diastereoisomer **12a** (*R*) (Fig. 3) revealed that Gibbs free energies are very similar (Fig. 4 and Table 1).

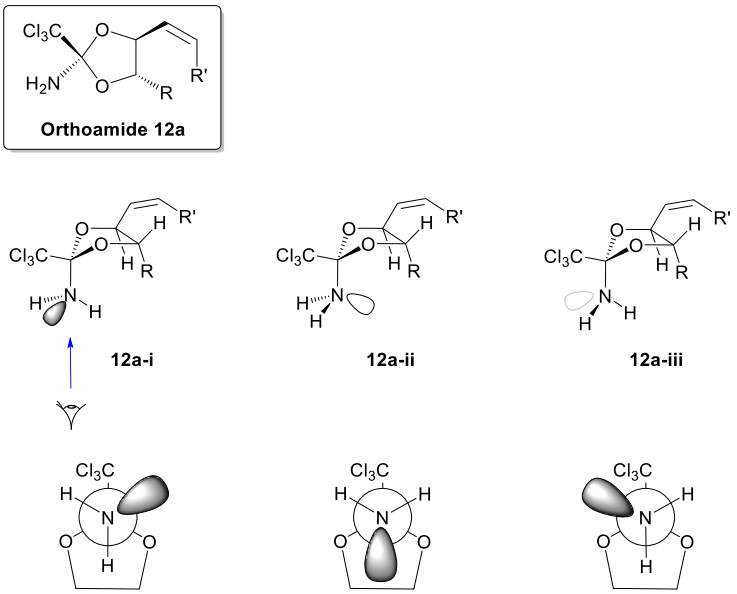

Fig. 3 Major staggered conformers of diastereoisomeric orthoamide **12a**.

Full geometry optimization has been conducted for the reactants. This was followed by a standard vibrational frequency to verify the nature of the stationary point (minimum or saddle point) and to obtain thermal contributions to Gibbs free energy at 1 atm and 453 K. Modern IGM analysis was performed to detect and quantify intramolecular interactions. To get a quick overview of the conformers of orthoamide diastereoisomers (**12a**), full geometry optimization has been carried out for the three most probable conformers. Several molecular conformations have been considered in each case, though only results for the most stable ones will be reported here (Fig. 4).

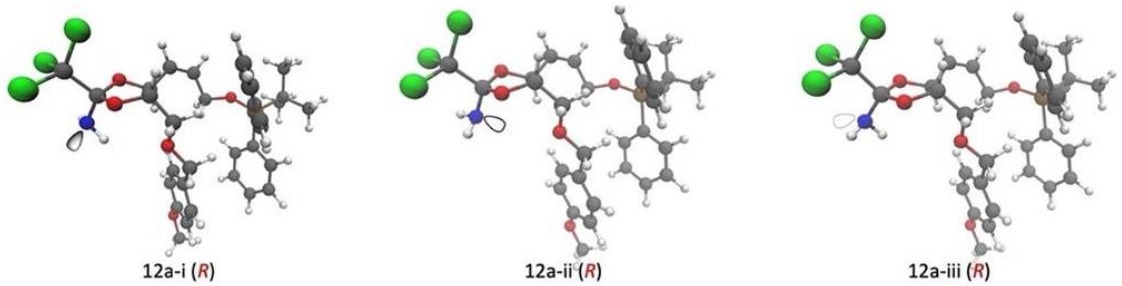

Fig. 4 Optimized structures (wB97X-D/Def2TZVP level) of the conformers of diastereoisomer **12a**.

Table 1. Computed Energies at wB97X-D/Def2TZVP (kcal.mol^{-1}) level and $d_{H(NH2)\cdots O(PMB)}$ (Å) for the diastereoisomer **12a**

		453K		$d_{H(NH2)\cdots O(PMB)}$
	Δ*E*	Δ*H*	Δ*G*	
12a-i	0.7	0.6	**-1.2**	2.890
12a-ii	0.2	0.1	**-1.0**	3.798
12a-iii	1.5	1.5	0.7	3.518

A first remark on this table is that the computed difference of Gibbs free energy (Δ*G*) is small and in some cases negligible (varying from -0.6 to 1 at 25 °C, and 0.7 to -1.2 at 180°C). Energies were obtained

in the range 298-447 K by using the KiSThelP program (S. Canneaux, F. Bohr, E. Hénon, *J. Comp. Chem.*, 2014, **35**, 82).

Nevertheless, this first theoretical consideration shows that **12a-i** and **12a-ii** are the most stable conformers of **12a**.

At this point of the discussion, it is important to detail the possible behaviors of the three conformers of orthoamide **12a**. The following figure emphasizes that the opening of the orthoamide can proceed according to two different ways leading to a “Dead end” imidate when the cleavage occurs on the C-O bond the closest to the double bond whereas the cleavage of the other C-O bond delivers the “Useful” imidate (Fig. 5).

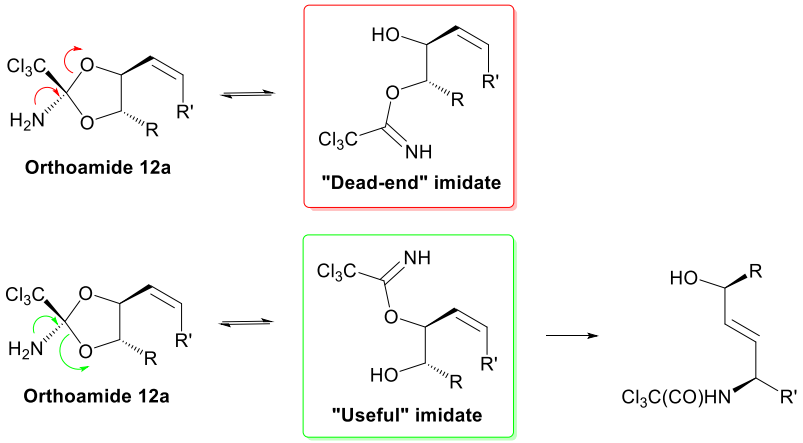

Fig. 5 Different openings of the orthoamide **12a**.

To meet favorable stereoelectronic requirements, there is a need for an antiperiplanar overlap between the non-binding N doublet and one of the C-O bond. It appears on figure 6, that only the most unstable **12a-iii** permits access to a productive imidate (even if interconversions between all conformers are clearly very rapid and solve this issue).

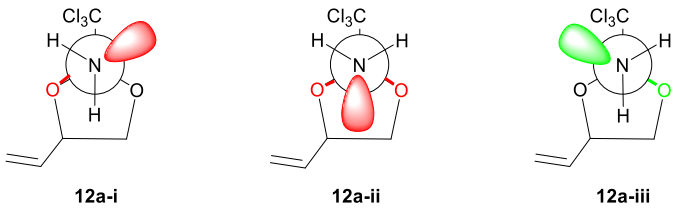

Fig. 6 Anti-periplanar overlaps and stereoelectronic requirements for a successful opening of orthoamide **12a**.

Then, the relatively recent IGM methodology was used in the hope of explaining the stabilization of **12a-i** (Fig. 7 and Fig. 8, the results being very similar for other conformers. C. Lefebvre, G. Rubez, H. Khartabil, J.-C. Boisson, J. Contreras-Garcia, E. Hénon, *Phys. Chem. Chem. Phys.* 2017, **19**, 17928; C. Lefebvre, H. Khartabil, J.-C. Boisson, J. Contreras-Garcia, J.-P. Piquemal, E. Hénon, *Chem. Phys. Chem.* 2018, **19**, 724; J. Klein, H. Khartabil, J.-C. Boisson, J. Contreras-Garcia, J.-P. Piquemal, E. Hénon, *J. Phys. Chem. A* 2020, **124**, 1850). This tool is particularly attractive to capture and characterize noncovalent interactions (the typical hydrogen-bond in the water dimer: δgpeak = 0.059 a.u. and the π -stacking present in the conformation of the benzene dimer: δgpeak = 0.009 a.u.). The strength of interaction was measured by the integration of δg (Δg).

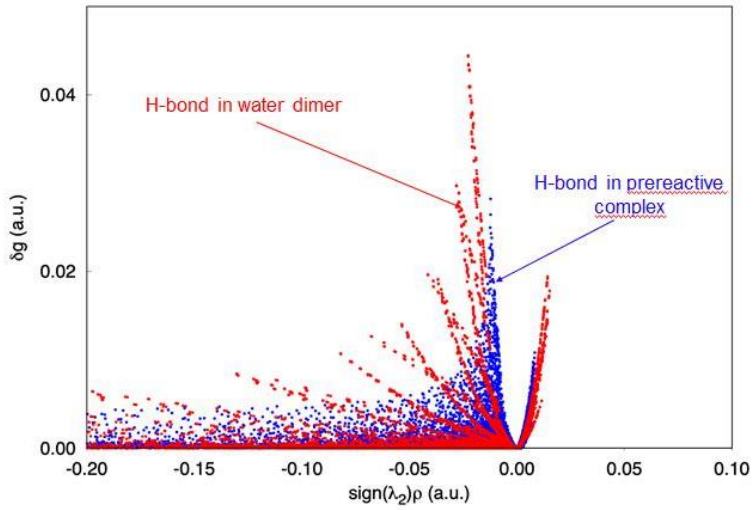

Fig. 7 Hydrogen-bond interactions δg signature revealed by the IGM approach in **12a-i**. Hydrogen-bond in the water dimer (red) is reported for comparison.

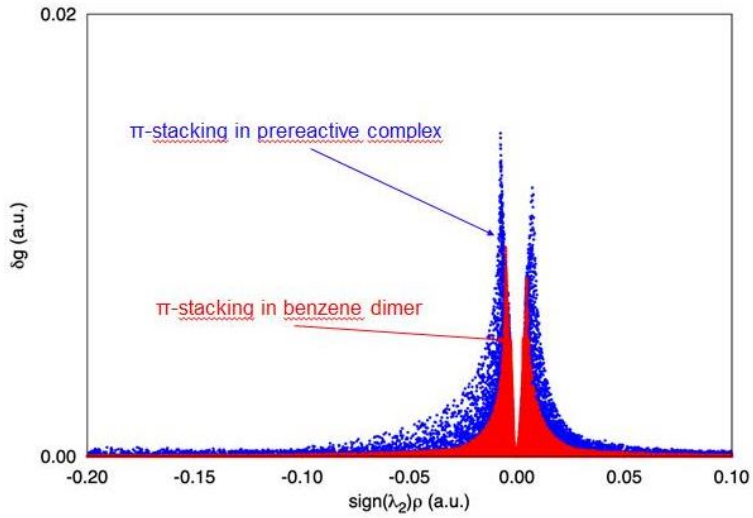

Fig. 8 π-stacking interactions δg signature revealed by the IGM approach in **12a-i**. π-stacking in the benzene dimer (red) is reported for comparison.

It appears from these results that a weak hydrogen bond exists (2.890 Å where usually 2.4-2.5 Å are observed) and that significant π-stacking interactions occur.

The second part of this theoretical study concerns the major staggered conformers (around the C-N bond) of diastereoisomer **12b** (*S*) (Fig. 9), showing once again very similar energies (Fig. 9 and Table 2).

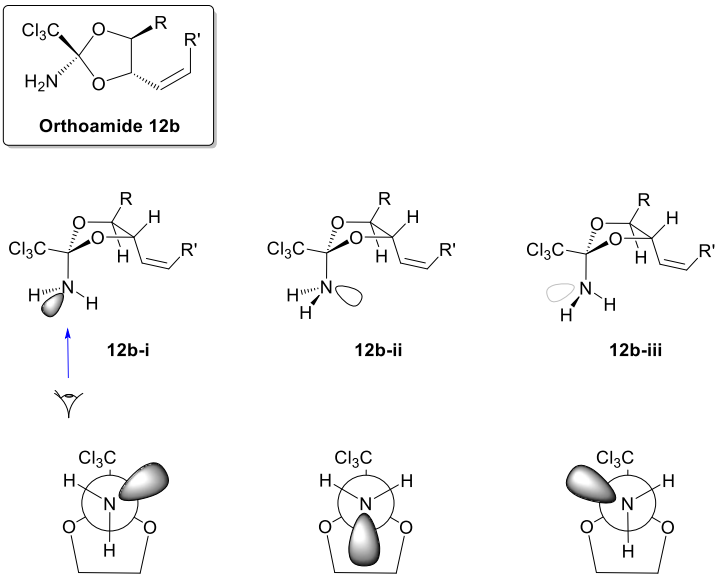

Fig. 9 Major staggered conformers of diastereoisomeric orthoamide **12b**.

To get a quick overview of the conformers of orthoamide diastereoisomers (**12b**), full geometry optimization has been carried out for the three most probable conformers. We have considered several molecular conformations in each case, though only results for the most stable ones will be reported here (Fig. 10).

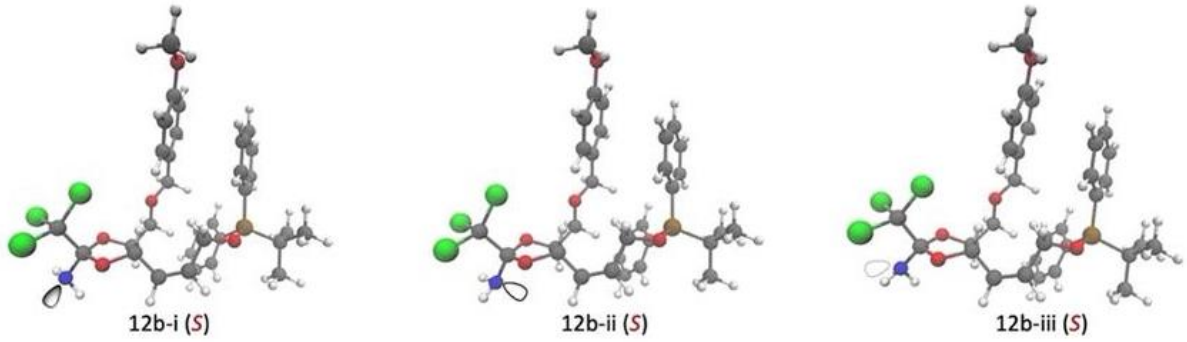

Fig. 10 Optimized structures (wB97X-D/Def2TZVP level) of the conformers of diastereoisomer **12b**.

Table 2. Computed Energies at wB97X-D/Def2TZVP (kcal.mol^{-1}) level for the diastereoisomer **12b**.

		453K	
	Δ*E*	Δ*H*	Δ*G*
12b-i	2.1	2.0	2.2
12b-ii	0.0	0.0	**0.0**
12b-iii	2.5	2.3	1.7

The first observation, by comparison of Tables 1 and 2, is that the diastereoisomer **12a** seems to be a little more stable than the diastereoisomer **12b**.

A second remark on this table is that the computed difference of Gibbs free energy (Δ*G*) is small and sometimes negligible (varying from 0.0 to 2.3 at 453K), showing that **12b-ii** is the most stable conformer of **12b**.

Interestingly, by comparison with figure 3, it is also necessary to cleave the C-O homoallylic bond and because positioning of substituent groups have been inversed between **12a** and **12b**, it results that the only favorable conformer should be **12b-i** (Fig. 11 and Fig. 12).

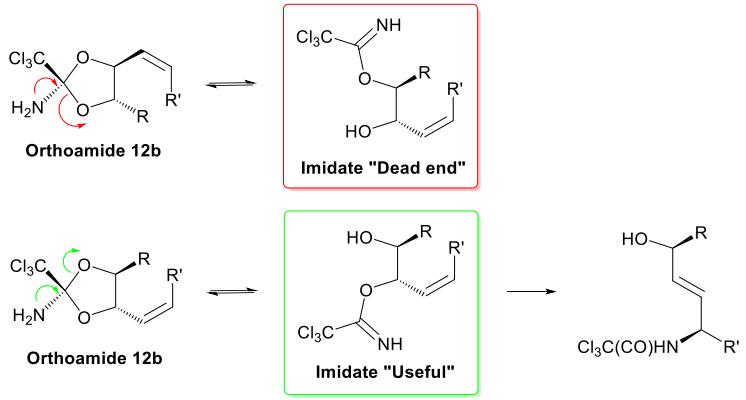

Fig. 11 Different openings of the orthoamide **12b**.

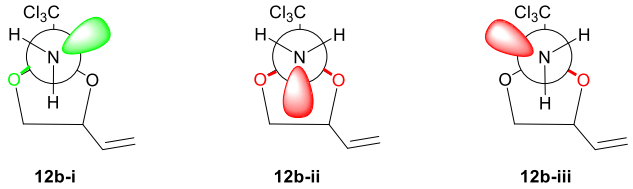

Fig. 12 Antiperiplanar overlaps and stereoelectronic requirements for a successful opening of orthoamide **12b**.

As an intermediate conclusion regarding the behaviors of orthoamides **12a** and **12b**, *a priori*, the different conformers have differences in energies, to a greater or lesser extent, and could react differently. Importantly, **12a-i**, **12a-ii** and **12b-ii** are the most stable ones, while **12a-iii** and **12b-i** are the most favorable ones for the formation of a “Useful” imidate in the Overman rearrangement, these parameters may slow down the process.

In order to determine the fractional equilibrium population for each of the six conformations represented in Fig. 4 and 10, free energies have been used assuming that they follow a Boltzmann distribution. As shown in Table 3 summarizing the results obtained, for the **12a** conformers, the **12a-i** is the strongly preferred (44.42 at 453K, 42.58 at 373K, and 39.64 at 298K), as one would expect due to steric reasons. It is also worth noting that in all of these compounds, the **12a** conformation is more favorable than the **12b** (**12a**/**12b** ratio: 86/14 at 453K, 85/15 at 373K, and 84/16 at 298K). We should mention that we have limited our analysis to the most stable conformations (the six ones represented in Fig. 4 and 10).

Table 3. Computed conformer percentages for the six conformations represented in Fig. 4 and 10.

Conformer	Population %		
	298K	373K	453K
12a-i	39.64	42.58	44.42
12a-ii	41.79	38.46	35.79
12a-iii	2.92	4.22	5.37
12b-i	0.42	0.73	1.06
12b-ii	14.64	12.91	11.65
12b-iii	0.58	1.10	1.70
12a/12b	84.36/15.64	85.26/14.74	85.59/14.41

B) Computation studies on prereactive complexes

The possibility of weakening of C-O bonds in the prereactive complex corresponding to the diastereoisomer **12a-i** (presumably giving a "Dead end" imidate) was investigated using Intrinsic Reaction Coordinate (IRC) calculations at the wB97X-D/Def2TZVP level considering that the conformers of **12a** are the most stable one (Fig. 13).

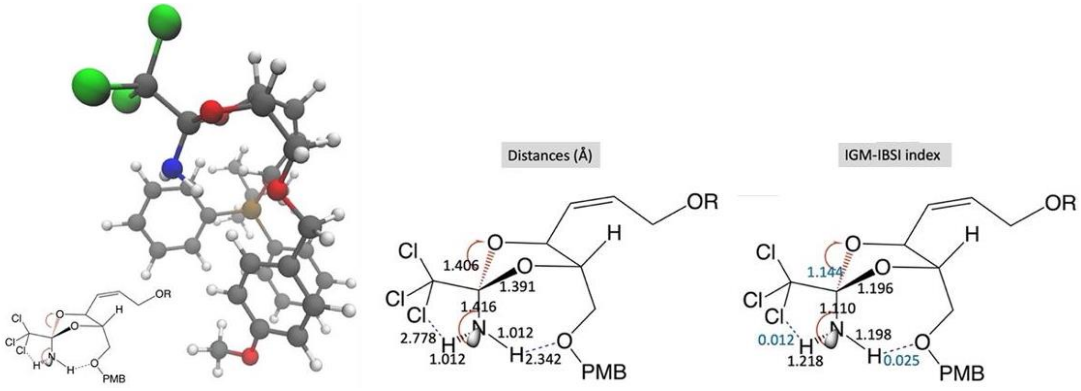

Fig. 13 Prereactive complex obtained from the endpoints of IRC calculations at the wB97X-D/Def2TZVP level for **12a-i**, and schematized structures with bond lengths and IGM-IBSI indexes.

This study revealed that one of the C-O bond is weaker (1.406 Å compared to 1.391 Å) with a lower IGM-IBSI index (1.144 compared to 1.196), meaning that this prereactive complex should evolve to cleave this weaker C-O bond, giving the "Dead end" imidate, with the imidate function positioned on an homoallylic place (unproductive for the Overman process). Note that in this prereactive complex, a complementary study showed interesting noncovalent interactions between the PMB group and the double bond side chain/TBDPS group (*R*), and hydrogen bonds between one chlorine atom and the NH, and between the OPMB and NH.

The same approach enabled us to study the weakening of C-O bonds in the prereactive complex corresponding to the diastereoisomer **12a-iii** (corresponding this time to the "Useful" imidate) also with IRC calculations at the wB97X-D/Def2TZVP level (Fig. 14).

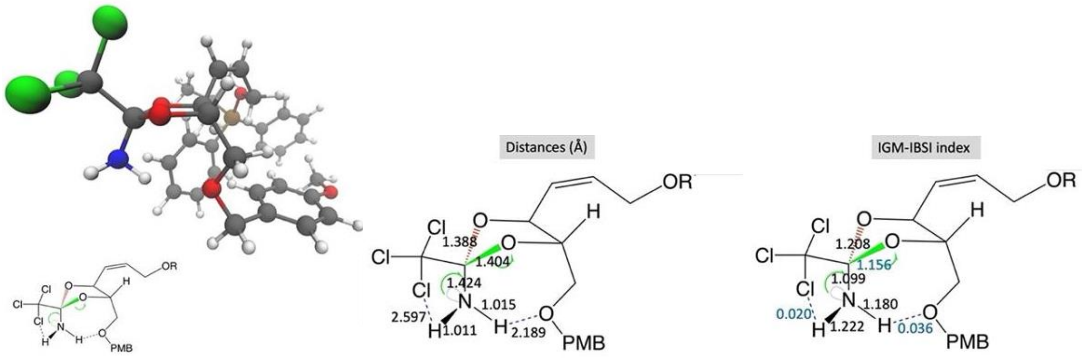

Fig. 14 Prereactive complex obtained from the endpoints of IRC calculations at the wB97X-D/Def2TZVP level for **12a-iii**, and schematized structures with bond lengths and IGM-IBSI indexes.

This study revealed that one of the C-O bond is weaker (1.404 Å compared to 1.388 Å) with a lower IGM-IBSI index (1.156 compared to 1.208), meaning that this prereactive complex should evolve to cleave this weaker C-O bond, giving the "Useful" imidate, with the imidate function positioned on an allylic place compared to the double bond (productive for the Overman process). Note that in this prereactive complex, a complementary study showed interesting noncovalent interaction between the PMB group and one phenyl of the TBDPS group (*R*), and hydrogen bonds between one chlorine atom and the NH, and between the OPMB and NH.
Interestingly, it seems that the prereactive complex resulting from the less stable conformer **12a-iii** is far more stable compared to the prereactive complex resulting from the most stable conformer **12a-i** (difference in ΔG at 453 K = 3.31 kcal.mol^{-1} (3.78 – 0.47), which is another parameter which may slow down the overall Overman process.

C) Computation studies on transition states

In the next part of this theoretical study, transition state structures (TS) have been located on the potential energy surfaces at the wB97X-D/Def2TZVP level using the Gaussian 16 program (M. J. Frisch *et al.* "Gaussian 16.", 2016). IRC analyses have been undertaken to examine the reaction path from the transition state structures of **12a** on a potential energy surface and to check the species connected by a transition state. Surprisingly, two reactants with the possible stabilizing hydrogen bond between NH_2 and OPMB have been obtained from the endpoints of IRC, which is in accordance with the hypothesis (Fig. 15).

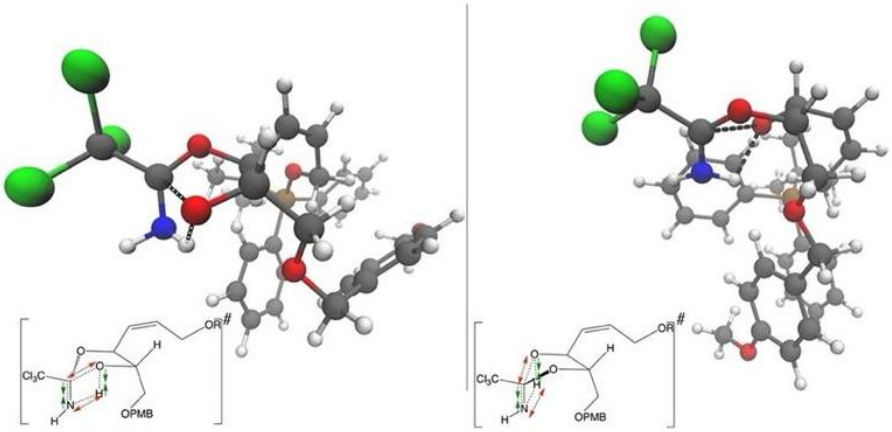

Fig. 15 Transition states structures TS1 and TS2 for **12a** orthoamide diastereoisomer at the wB97X-D/Def2TZVP level.

The transition state TS1 – that leads to an imidate on allylic position – has shorter distances for the C-O broken bonds (2.36 Å *vs* 2.57 Å) and the H-O being formed bonds (1.68 Å *vs* 1.99 Å) than the distances of the transition state TS2 – that leads to an imidate on homoallylic position. In the last case (TS2), the C-N distance is shorter (1.29 Å *vs* 1.33 Å); this case looks like a semi-planar transition state (Table 3).

Table 3. Lengths for the bonds being formed and broken in the transition structures of Fig. 14 and relative energies (kcal.mol^{-1}) for **12a**.

	Lengths (Å)				298K		
	O…C	N…H	O…H	C-N	Δ*E*	Δ*H*	Δ*G*
TS1	2.361	1.065	1.677	1.325	0.00	0.00	0.00
TS2	2.570	1.028	1.988	1.292	5.73	5.76	4.86

Some additional computations were also performed to accurately predict the barrier of the two reactions, leading to the imidate product substitutions on allylic and on homoallylic positions (Fig. 16 and Table 4). The computed Gibbs free energies for these reactions ΔG°‡ are 49.2 and 54.1 kcal.mol^{-1} for **12a-i** and **12a-iii** respectively. These (high) free energy barriers may explain why elevated experimental temperature is required in this Overman process.

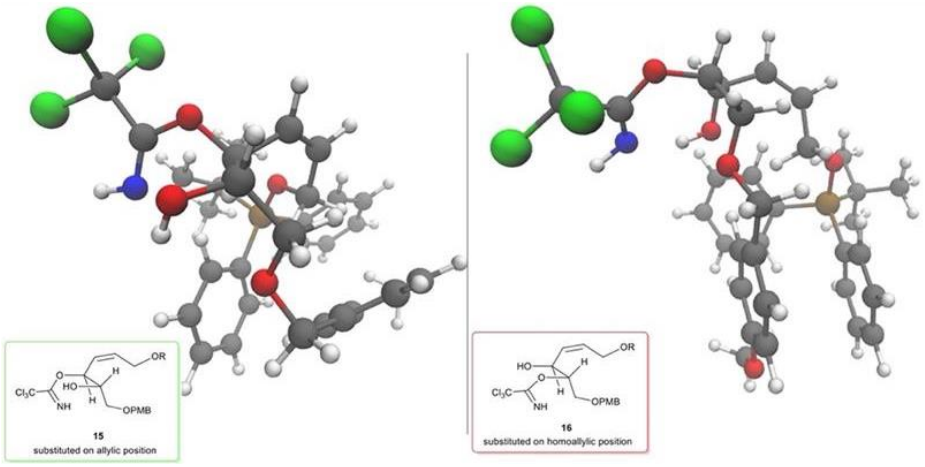

Fig. 16 The imidates **15** and **16** obtained from the endpoints of IRC calculations at the wB97X-D/Def2TZVP level.

Table 4. Energies for the species involved in the reaction at 298 K (wB97X-D/Def2TZVP level).

	ΔUp	$\Delta H°_{298\,K}$	ΔG°
12a-i	49.7	47.5	49.2
12a-iii	55.5	53.3	54.1

D) Attempted energy profile for the formation of imidates

Based on all the results obtained by these theoretical calculations, an energetic profile was proposed for the formation of the imidates (Fig. 17).

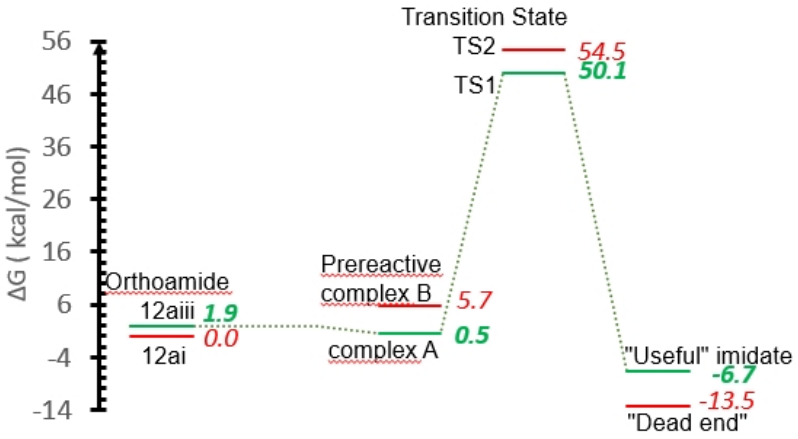

Fig. 17 Gibbs free energy scheme with all the measured values in the case of **12a-i** and **12a-iii** evolutions.

E) Overall conclusions to explain the problematic formation of imidates in the overall Overman process

- The different conformers of orthoamides have differences in energies, to a greater or lesser extent, and can react differently. Importantly, **12a-i**, **12a-ii** and **12b-ii** are the most stable ones. In terms of formation of a "Useful" imidate, **12a-iii** and **12b-i** are the most favorable ones, and overall all these parameters may slow down the process.
- The prereactive complex resulting from the less stable conformer **12a-iii** is far more stable compared to the prereactive complex coming from the more stable conformer **12a-i**, which is another parameter which may slow down the overall Overman process.
- The computed Gibbs free energies for the reactions $\Delta G°‡$ are equal to 49.2 and 54.1 kcal.mol^{-1} for **12a-iii** and **12a-i** respectively. These (high) Gibbs free energy barriers may explain elevated experimental temperature conditions.